Structural elucidation upon binding of antimicrobial peptides into binary mixed lipid monolayers mimicking bacterial membranes

DOI:
10.1016/j.jcis.2021.04.037

Document Version
Accepted author manuscript

Journal of Colloid and Interface Science 598 (2021) 193–205

Structural elucidation upon binding of antimicrobial peptides into binary mixed lipid monolayers mimicking bacterial membranes

Daniela Ciumac[1], Haoning Gong[1], Richard A. Campbell[2,3], Mario Campana[4], Hai Xu[5] and Jian R. Lu[1,*]

[1] Biological Physics Laboratory, School of Physics and Astronomy, University of Manchester, Oxford Road, Schuster Building, Manchester M13 9PL,

[2] Institut Laue-Langevin, 71 Avenue des Martyrs, CS-20156, 38042 Grenoble, France

[3] Division of Pharmacy and Optometry, University of Manchester, Oxford Road, Stopford Building, Manchester M13 9PT.

[4] ISIS Neutron Facility, STFC, Chilton, Didcot OX11 0QZ, UK

[5] Centre for Bioengineering and Biotechnology, China University of Petroleum, Qingdao, China

* To whom all correspondence should be made; Tel: +44 161 2003926; Email: j.lu@manchester.ac.uk

Keywords: Antimicrobial peptides, bacterial membrane, lipid monolayer, bactericidal, membrane-lytic, neutron reflection, Langmuir film, membrane binding.

Abbreviations: AMP, antimicrobial peptide; CL, cardiolipin; DPPE, 1,2-dipalmitoyl-sn-glycero-3-phosphoethanolamine; DPPG, 1,2-dipalmitoyl-sn-glycero-3-phospho-(1'-rac-glycerol); LC, liquid-condensed; LE, liquid-expanded; MIP, maximum insertion pressure; NR, neutron reflectivity/reflectometry/reflection; NRW, null reflective water; PBS, phosphate buffered saline; PE, phosphatidylethanolamine; PG, phosphatidylglycerol; POPG, 1-palmitoyl-2-oleoyl-sn-glycero-3-phospho-(1′-rac-glycerol); S, solid; SLD, scattering length

density; TMCL, tetramyristoylcardiolipin (with 1',3'-bis[1,2-dimyristoyl-sn-glycero-3-phospho]-sn-glycerol being actually used).

Abstract

Hypothesis

Antimicrobial peptides (AMPs) kill microorganisms by causing structural damage to bacterial membranes. Different microorganisms often require a different type and concentration of an AMP to achieve full microbial killing. We hypothesise that the difference is caused by different membrane structure and composition.

Experiments

Given the complexities of bacterial membranes, we have used the binary DPPG/TMCL to mimic the cytoplasmic membrane of Gram-positive bacteria and the binary DPPG/DPPE to mimic the cytoplasmic membrane of Gram-negative bacteria, where DPPG, TMCL and DPPE stand for 1,2-dipalmitoyl-sn-glycero-3-phospho-(1'-rac-glycerol), 1',3'-bis[1,2-dimyristoyl-sn-glycero-3-phospho]-sn-glycerol, and 1,2-dipalmitoyl-sn-glycero-3-phosphoethanolamine, respectively. A Langmuir trough was specially designed to control the spread lipid monolayers and facilitate neutron reflectivity measurements.

Findings

Surface pressure-area isotherm analysis revealed that all binary lipid systems mix non-ideally, but mixing is thermodynamically favoured. An increase in the surface pressure encourages demixing, resulting in phase separation and formation of clusters. Neutron reflectivity measurements were undertaken to study the binding of an antimicrobial peptide $G(IIKK)_4$-I-NH_2 (G_4) to the binary DPPG/TMCL and DPPG/DPPE monolayer mixtures at the molar ratios of 6/4 and 3/7, respectively. The results revealed stronger binding and penetration of G_4 to the DPPG/TMCL monolayer, indicating greater affinity of the antimicrobial peptide due to the electrostatic interaction and more extensive penetration into the more loosely packed lipid film. This work helps explain how AMPs attack different bacterial membranes, and the results are discussed in the context of other lipid models and antibacterial studies.

1. Introduction

The worldwide increase of antimicrobial resistance to traditional antibiotics has put tremendous pressure on global healthcare. Whilst many countries and organisations have recommended various measures in order to regain the control over microbial infections, one of the urgent actions is to develop new antibiotic agents with different or improved mechanisms of action [1, 2]. Antimicrobial peptides (AMPs) have attracted considerable attention in this regard because they kill bacteria by causing fast and irreversible structural disruptions to microbial membranes. This mode of action is physical and does not involve any specific biochemical, enzymatic, metabolic or genetic process, thus holding great potential for the development of new medicines in the fight against infections, especially those caused by multi-drug resistant bacteria [3, 4].

A predominant factor underlying the efficacy and cell selectivity of positively charged AMPs lies in the different composition and morphology of microbial membranes, the target for the physical structure disruptions. In the case of bacteria, the anionic lipids are readily exposed on the outer surface of their membranes, while in mammalian cells they are largely imbedded in the inner leaflet of the membrane (e.g., the membrane of human red blood cells contains up to 0.7% of anionic lipids in the outer leaflet and up to 9% in the inner leaflet) [5]. This means that the outer membrane surface remains largely neutral. Thus elucidating how AMPs interact with specific membrane lipids can help improve their rational design as novel peptide antibiotics by maximizing their potency whilst minimizing their cytotoxicity [6-8].

Gram-negative (G-) bacteria such as *Escherichia coli* are usually surrounded by two membranous bilayers, with the inner one (the plasma membrane) being composed of phospholipids and the outer membrane bilayer consisting of proteins, including porins, receptors, and an asymmetric distribution of lipids. The outer leaflet of the outer membrane primarily contains negatively charged lipopolysaccharides projecting outside and the inner leaflet contains phospholipids and lipoproteins. The two bilayers are connected by an intermediate periplasmic layer containing the peptidoglycan. In contrast, whilst Gram-positive (G+) bacteria such as *Staphylococcus aureus* are also covered by the cytoplasmic membrane bilayer, they do not have the outer membrane lipid bilayer. Instead, they build their outer cell wall from many peptidoglycan layers of about 40–80 nm thick. Thus, the total cell wall of G+ bacteria is drastically thicker than that of G- bacteria with a total thickness just about 7-8 nm incorporating a single layer peptidoglycan only [9].

Outer membrane lipids such as LPS (lipopolysaccharides) on the outer membrane surface of G- bacteria and LTA (lipoteichoic acids) on the outer membrane surface of G+ bacteria carry multiple negative charges as well as long acyl chains. They work as the first line of defence against incoming AMPs carrying positive charges. Charge driven electrostatic interaction coupled with subsequent hydrophobic interaction imposes structural disruptions to the outer defence line. Once compromised, some AMPs manage to reach the inner plasma membrane to impose the lethal killing by causing leakage of the inner contents. Whilst some aspects of the sequential events have been supported by experimental observations, there is still a lack of convincing details at the nanometre scale to support such hypothesis. There is however some consensus about how selective binding of an AMP to the inner and outer membranes affects its antimicrobial efficacy [7].

Extensive effort has been devoted to mimic the delicate bilayer structures of cells, both of eukaryotes and prokaryotes, but fabrication of membrane bilayers incorporating appropriate membrane composition still represents a major area of challenges in membrane research [10-12].Whilst the overall composition of cytoplasmic membranes varies between different bacterial types, the main anionic lipid components are phosphatidylglycerol (PG), and cardiolipin (CL), with the predominant zwitterionic lipid being phosphatidylethanolamine (PE) [13, 14]. All bacteria have at least 15% of anionic lipids, either PG or CL, or a combination of both, while G- bacteria contains a higher amount of PE than G+ bacteria. The major phospholipid contents in the membranes of *E. coli* are 70-80% PE, 15-20% PG and 0-5% CL [15, 16]. Moreover, bacteria can alter their membrane composition and properties depending on the mitotic state, as a response to various environmental conditions [17], as well as to exposure to antibiotics [18]. The main anionic membrane lipid contents of *S. aureus* are 50-60% PG and 40-50% CL [19], but the bacteria can also alter its PG to CL ratio when the cells enter the stationary phase by increasing the CL content at the expense of PG [20]. Therefore, a comprehensive characterisation of bacterial membrane composition would provide important information regarding the role of lipid packing and composition in modulating the properties of bacterial membranes.

Malanovic et al [9], Epand et al [21] and others [22-24] have shown that changes in lipid membrane composition affect the sensitivity of various bacteria to antimicrobials [21] and that phospholipids can also become involved in the action of AMPs. It is thus important to construct different membrane mimicking models to investigate how changes in membrane composition affect how different membrane active molecules attack cell membranes. In this

respect, spread lipid monolayer systems as controlled by Langmuir trough can provide useful information on the interactions between AMPs and model monolayers mimicking the membranes of different microorganisms, whilst allowing the precise control of temperature, lateral packing, and composition [25, 26]. Moreover, the thermodynamic relationship between monolayer and bilayer models is direct [27], with the assumption that a bilayer can be considered as two weakly coupled monolayers [28]. These features make spread Langmuir monolayers a very useful platform to study the characteristics of bacterial membrane structures as well as the interaction between lipids and AMPs. For example, using a monolayer model from PE/eggPG/CL (78/4.7/14.4) to mimic the *E. coli* cytoplasmic membrane, Zhang et al. [29] have studied the interaction of several natural and synthetic AMPs with this mixture as well as the individual monolayer constituents. Increasing AMP concentration often causes a sigmoidal increase in the surface pressure of the mixture, indicating a cooperative interaction of the AMP molecules with the lipid monolayer. In another study, using single and binary component mixtures, Sevcsik et al. [30] showed that the membrane-disruptive activity of LL-37 was influenced not only by the lipid charges, but also by other parameters, such as the packing density, formation of intermolecular hydrogen bonding and lipid molecular shape.

In a previous study, we have assessed the implication of lipid monolayer charges on their interaction with a rationally designed helical AMP, i.e., $G(IIKK)_4I\text{-}NH_2$ (G_4) [31]. By combining surface pressure measurements, neutron reflection (NR) and Brewster angle microscopy, we showed that whilst G_4 was associated only with the head groups of the dipalmitoyl-PC (DPPC) monolayer, it was able to penetrate the lipid acyl chain region of dipalmitoyl-PG (DPPG) monolayer, concomitant with the removal of some lipid molecules from the interface. These results, when considered in the context of the general antibacterial action mechanism of cationic AMPs, showed that the combined effect of the initial electrostatic interaction followed by the subsequent hydrophobic interaction led to the increased power of G_4 in disrupting the charged membranes. A further study investigated how lipid packing and acyl chain saturation influenced the binding of the G_4 peptide onto model lipid monolayers comprised of saturated DPPG and unsaturated 1-palmitoyl-2-oleoyl-sn-glycero-3-phospho-(1′-rac-glycerol) (POPG, sodium salt). The results revealed the clear impact on the amount and distribution of G_4 into different parts of the model lipid monolayers [32]. However, these previous studies have used very simplified membrane leaflet models consisting of single lipids. In order to have a more realistic insight into G_4

selectivity characteristics when binding onto different types of cell membranes, more complex model monolayers must be used to represent key lipid compositions.

In this work, we have created two binary mixtures, DPPG and TMCL in a 6:4 molar ratio to mimic the membrane composition of G+ bacteria (e.g. *S. aureus*), and DPPG and DPPE in a 3:7 molar ratio to mimic that of G- inner membrane composition (e.g. *E. coli*). The aim of this study is to perform a comprehensive analysis of these monolayers and to characterise their interaction with the G_4 peptide. The first two parts of the work are dedicated to surface pressure-area isotherms and an analysis of the interactions between the lipid constituents in the mixtures by analysing the thermodynamic parameters. The last two parts consist of kinetic, compositional and equilibrium structural studies on the binding selectivity of G_4 to the two model mixtures comprised of DPPG/TMCL and DPPG/DPPE by neutron reflection.

2. Materials and Methods

2.1 Materials

All the lipids were purchased from Avanti Lipids (Alabaster, AL) and were used without further purification (purity as received > 99%). Tail-deuterated DPPG, d_{62}-DPPG, (1,2-dipalmitoyl-d62-sn-glycero-3-phospho-rac-(1-glycerol), sodium salt), hydrogenous DPPG (1,2-dipalmitoyl-sn-glycero-3-phospho-(1'-rac-glycerol), sodium salt), hydrogenous DPPE (1,2-dipalmitoyl-sn-glycero-3-phosphoethanolamine), and hydrogenous TMCL were dissolved in chloroform/methanol (9:1 v/v) mixture (both chloroform and methanol were purchased from Sigma-Aldrich, HPLC grade, ≥99.9%). TMCL stands for tetramyristoylcardiolipin, with 1',3'-bis[1,2-dimyristoyl-sn-glycero-3-phospho]-sn-glycerol (sodium salt) being used in this work and denoted as 14:0 cardiolipin, or 14:0 CL. Stock solutions were prepared to a concentration of 2 mM. The binary lipid mixtures were prepared from the stock solutions using a Hamilton syringe to ensure accuracy. The buffer solution used as subphase contained 10 mM PBS (phosphate buffered saline, 10 mM, 137 mM NaCl, pH/D = 7.4) and prepared from tablets (Sigma-Aldrich), with either UHQ (Elgastat ultrapure water) grade water (18 MΩ·cm), or D_2O (Sigma-Aldrich). Peptide $G(IIKK)_4I\text{-}NH_2$ (G_4) was supplied by Shanghai TopPeptide Bio Co Ltd with >98% purity and was synthesized using the standard Fmoc method, with the method previously described by Hu et al. [33] and was used as received. G_4 is composed of 18 amino acids, and has a positive net charge of +9 (at

neutral pH). The peptide stock solution (0.2 mM) was also prepared in PBS solution. All the experiments were performed at the room temperature of 21 ± 1 °C.

2.2 Surface pressure measurements

Surface pressure measurements of AMP−lipid interactions were carried out on a specially designed Langmuir trough, to facilitate NR experiments (Nima Technology Ltd., Coventry, UK), with all the lipid monolayers prepared as previously described [32]. Briefly, after thoroughly cleaning the trough, and filling it with 80 ml of PBS solution, the monolayer was prepared by spreading the lipids on the subphase. Following solvent evaporation and monolayer equilibration, the surface pressure-area isotherms (π-A) were recorded by compressing the barrier at a speed of 5 cm^2/min. All the π-A measurements were repeated in triplicate, in order to ensure the reproducibility. For the peptide biding experiments, we used the constant area method. After the monolayer was compressed to the required surface pressure, the barrier position was fixed. After monolayer equilibration, the peptide solution was slowly injected via a 10-cm bent needle from the stock solution, to a final concentration in the subphase of 3 μM. Then the surface pressure changes over time as a result of peptide penetration were recorded for a period of at least 120 min.

2.3 Analysis of π-A isotherms

In order to gain insight in the properties of the binary lipid mixtures containing either DPPG/TMCL or DPPG/DPPE, we performed a thermodynamic analysis under three representative surface pressures, at 8, 15 and 28 mN/m. Firstly, from the slope of the π-A isotherms, the compressibility modulus, Cs^{-1} (mN/m), can be calculated using the following equation;

$$C_s^{-1} = -A\left(\frac{d\pi}{dA}\right) \quad (1)$$

where A is the mean area per lipid molecule at surface pressure π [34]. The compressibility modulus gives information about the molecular ordering of the lipid film. It is zero for a clean surface and increases with the amount of surface-active material present at the interface. Bigger compression modulus values correspond to less compressible membrane.

Furthermore, the excess area of mixing, ΔA_{ex} ($Å^2$/molecule), can be calculated by comparing the mean molecular areas of the mixture with those of the unmixed components at the same surface pressure, according to the following equation:

$$\Delta A_{ex} = A_{1,2} - A_{id} = A_{1,2} - (x_1 A_1 + x_2 A_2) \quad (2)$$

where $A_{1.2}$ is the mean molecular area in the mixed monolayer at a given surface pressure; A_{id} is the mean area per lipid molecule for an ideal mixed monolayer (with two components), expressed as a linear addition of the individual components; A_1 and A_2 are the respective molecular areas in the single-component monolayer of components *1* and *2* at the same surface pressure; x_1 and x_2 are the respective mole fractions of the components in the mixed monolayer. If the mixing of molecules is ideal or the two components are immiscible, ΔA_{ex} = 0, the plot is linear [35]. Deviations from these conditions indicate miscibility or non-ideality. Positive deviations indicate the presence of repulsive interactions between different molecules in the mixed monolayer (leading to expansion), whereas negative deviations suggest attractive interactions leading to condensation [36].

In order to obtain quantitative information on intermolecular forces in the mixed films the excess Gibbs energy of mixing, ΔG_{ex}, was determined according to the following equation:

$$\Delta G_{ex} = \int_0^{\pi} \Delta A_{ex} d\pi \quad (3)$$

where ΔG_{ex} (J/mol) represents the contribution of mutual interactions between molecules on the free energy change of mixing and indicates the extent of stability upon mixing. The negative sign ΔG_{ex} signifies stable monolayer (attractive interaction), while a positive value suggests phase separation in the monolayer, (i.e., the interaction upon mixing is more repulsive than in constituent one component monolayers) [36].

In order to further examine the properties of the binary component monolayers upon mixing, the total free energy of mixing, ΔG_{mix}, was calculated from the following equation:

$$\Delta G_{mix} = \Delta G_{id} + \Delta G_{ex} \quad (4)$$

where ΔG_{id} (J/mol) is the ideal free energy change of mixing for the binary mixture as referred to in this work. It is only related to entropy and can be evaluated from:

$$\Delta G_{id} = RT(x_1 \, ln \, x_1 + x_2 \, ln \, x_2) \quad (5)$$

where R is the gas constant (J/mol/K) and T is the temperature (K). The negative value of the total energy of mixing, G_{mix}, proves that the two-dimensional (2D) mixed state is thermodynamically more stable than the corresponding unmixed state [35].

2.4 Neutron reflection (NR)

The NR measurements of the lipid monolayers were carried out on FIGARO at the Institut Laue-Langevin (Grenoble, France) [37], and on INTER of Target Station 2 and SURF of Target Station 1 at the STFC Rutherford Appleton Laboratory (Chilton, Oxfordshire, UK). Measurements of neutron reflectivity, *R(Q)*, were obtained as a function of momentum transfer, *Q*, ($Å^{-1}$, $Q = 4\pi sin\theta/\lambda$, where λ is the neutron wavelength and θ is the beam incidence angle). The time-of-flight FIGARO instrument was used with a chopper pair, giving a wavelength range between 2 and 30 Å. The data were acquired at two incident angles of 0.62° and 3.8°, giving a *Q* range from about 0.005 to 0.4 $Å^{-1}$. The background was subtracted using a 2D detector. On INTER, the measurements were made with two incident angles of 0.8° and 2.3°, giving a *Q* range from 0.014 to 1 $Å^{-1}$. On SURF the data were collected using either two angles (0.65° and 1.52°) or one angle (1.52°). All the instruments were calibrated using a pure D_2O subphase. For the DPPG/TMCL system, the measurements were done using 4 isotopic contrasts of h-DPPG/h-TMCL and d-DPPG/h-TMCL in either D_2O or NRW (null reflective water, 8.1% D_2O in H_2O, SLD=0). Equivalent 4 contrasts were also recorded for the DPPG/DPPE system. The NR experiments were conducted under the same experimental conditions as for the surface pressure measurements. Two different implementations of the experiments were performed.

First, a dynamic compositional analysis was performed during the interaction of G_4 with the mixed lipid monolayers at the initial surface pressures of 15 mN/m. The low-*Q* analysis approach of FIGARO was used to follow the compositional changes over time [38, 39]. Dynamic changes in the composition of a binary mixture during antimicrobial peptide binding were measured on a Langmuir trough facilitating neutron reflection [40, 41], using the low-*Q* analysis method that was applied in our previous work to resolve kinetic compositions for the first time during the binding of G_4 peptide to saturated lipid monolayers of different charges [31]. Reflectivity data used were only in the *Q* range 0.01–0.03 $Å^{-1}$ where the details of the actual interfacial structure had minimal influence on the model. In order to follow the process of peptide binding in real time, reflectivity data were recorded at the incident angle of 0.62° for both hydrogenous (hDPPG/hTMCL and hDPPG/hDPPE) and deuterated (dDPPG/hTMCL and dDPPG/hDPPE) lipid monolayers on the surface of NRW, before and after injecting the G_4 peptide. In each case, kinetic data during the interaction were recorded every 4 min for the former contrasts with the scattering contribution of the latter contrast interpolated from the equilibrium values before and after the interaction. For each system, the low-*Q* analysis method functions as follows: the difference in scattering

between the two contrasts resolves the surface concentration of DPPG, the surface concentration of the other lipid is constrained from the stoichiometry of the spread lipid monolayer, and the absolute scattering of the other contrast reveals the surface concentration of peptide. In practice, following careful calibration of the background using pure NRW data, we applied a single layer model to the reflectivity data recorded in both isotopic contrasts on NRW, and then used the following equation to calculate the surface concentration of each component:

$$\rho\tau = N_A\left(\Gamma_{lipid}b_{lipid} + \Gamma_{peptide}b_{peptide}\right) = \left(\frac{b_{lipid}}{A_{lipid}} + \frac{b_{peptide}}{A_{peptide}}\right) \quad (6)$$

where ρ is the fitted scattering length density ($Å^{-2}$), τ is the nominal thickness (Å), N_A is the Avogadro's number, Γ is the surface concentration (mol/m^2), A is area per molecule ($Å^2$) and b is the scattering length (Å) for the lipid and peptide components, respectively. The batch fit function of Motofit was used [42]. In order to apply Eq. 6 to calculate the surface concentrations of the peptide and the lipid mixture over time, we measured reflectivity profiles against time by subjecting each h/h lipid mixture monolayer to G_4 binding. In addition, reflectivity profiles were measured from each d/h lipid mixture just before addition of G_4 and then after its binding equilibrium. As explained previously, this contrast does not offer reliable information about the dynamic binding of G_4 because of the high value of scattering length from the d/h lipid [31]. However, the limited data measured from the d/h lipid runs helped us to extract dynamic changes in the concentrations of both lipid mixture and G_4 from the low-Q data analysis [40,41], with the procedures adopted in the low-Q data analysis further described in Section S4 of the Support Information.

Second, an equilibrium structural analysis was performed before and after the binding of G_4 with the mixed lipid monolayers at the initial surface pressures of 8, 15 and 28 mN/m. Data recorded over the full Q range in all 4 isotopic contrasts were fitted to a stratified layer model, again using Motofit based on optical matrix formalism [43] to fit the Abeles layer model to the interfacial structure [44]. The model which fitted the data with the least number of layers was considered to be the most appropriate one. For the lipid only systems, a two-layer model was fitted, with the 1st layer being associated with the tail region and the 2nd with solvated head groups. After the peptide was injected and the system reached equilibrium, the interfacial structure was fitted following the same approach, using either the two-layer model, with the peptide associated with both the tails and the solvated head groups of the lipid

monolayer, or a three-layer model, where in addition to being associated with the tails and head groups, the peptide was also bound under the monolayer. The amount of each component can be calculated from the following equation:

$$\rho_{fit} = \rho_{lipid}\varphi_{lipid} + \rho_{peptide}\varphi_{peptide} + \rho_{solvent}\varphi_{solvent} \quad (7)$$

where ρ_{fit} is the fitted scattering length density (SLD) value of the layer, ρ_{lipid}, $\rho_{peptide}$, and $\rho_{solvent}$ are the respective calculated SLD values of the lipids (tails or heads), peptide and solvent, and φ_{lipid}, $\varphi_{peptide}$, and $\varphi_{solvent}$ denote their respective volume fractions. The total volume fraction for each layer of lipid, peptide, and solvent components is equal to unity.

The mean area per molecule, A (Å^2), for each component, can be calculated as:

$$A = \frac{\sum b}{\tau\rho\varphi} \quad (8)$$

where Σb is the sum of the atomic scattering lengths of the respective component, τ the fitted layer thickness, and ρ and φ its calculated SLD and volume fraction. Note that the area per molecule of the chains and the head groups were constrained in the fitting process to be the similar. After calculating the areas per molecule of each component, their respective surface concentration, Γ, can be calculated as:

$$\Gamma = \frac{1}{AN_A} \quad (9)$$

The molecular volume and SLD values of the peptide were computed using Biomolecular SLD Calculator developed by ISIS Neutron Facility (http://psldc.isis.rl.ac.uk/Psldc/). The scattering lengths, SLD values and molecular volumes of individual lipid components and G_4 are summarized in Table S1a. Because we didn't have deuterated TMCL and DPPE, it is impractical to solve the surface concentrations of each lipid in a binary mixture. Thus, all the NR experiments were treated as having 2 components, lipid and peptide G_4. The lipid here denotes each binary mixture with b and ρ being calculated as the average of respective molar ratio of the two lipids in each mixture. The detailed parameters for each pair of binary lipid mixtures in hydrogenous and deuterated forms are shown in Table S1b. Moreover, it was assumed that the lipids in the mixture maintained their molar ratios during the interaction with the peptide.

3. Results and discussion

3.1 Thermodynamic properties of binary mixtures

The main differences between PG, CL and PE relate to their charges and their molecular shape (Fig. S1). At physiological pH values PG and CL are negatively charged, while PE is zwitterionic. The PE lipid has a smaller cross-sectional area of the head group than that of the acyl chains and is inverted cone-like, therefore being prone to form non-planar lipid aggregates. Moreover, due to hydrogen bonding through their ionisable amines, PE lipids are prone to dense lipid packing [45]. The PG molecule has similar cross-sectional areas from its head and tail regions and can be described as a cylinder. However, because of the charge on the head group, the PG lipid can occupy a larger molecular area than what is predicted from its molecular shape. Due to the electrostatic repulsion it often results in loose packing [46]. In contrast, CL is a unique dimeric phospholipid consisting of two phosphatidic acids linked up by a glycerol, thus carrying four acyl chains in the same molecule [47]. At the physiological pH, CL has only one negative charge, but under certain conditions it can carry two negative charges (pK_1 = 2.8, pK_2 > 7.5) [48]. The smaller cross-sectional area of the head group against that of acyl chains of CL gives an inverted truncated cone shape to the lipid molecule. Depending on the pH and ionic strength of the environment, CL molecules have the propensity to form non-lamellar lipid phases, which can be attenuated by the presence of repulsive negative charges of the head groups, but promoted in the presence of divalent cations [49]. Therefore, in designing an experiment involving lipids mimicking various membranes, the lipid specificity of the system has to be taken into account. Moreover, when studying the behaviour of these lipids, the aqueous environment conditions are very important, as processes such as lipid-ion interactions can influence the packing and behaviour of the monolayers [50, 51].

In order to undertake the thermodynamic analysis of the DPPG/TMCL and DPPG/DPPE monolayers, we measured π-A isotherms of pure lipid and their binary mixed films as a function of DPPG molar fraction. The results show that in the case of DPPG/TMCL mixing (Fig. 1a), both DPPG and TMCL alone and their mixtures present well defined phase transitions from liquid-expanded (LE) phase over the low surface pressure region, followed by a coexistent region of the LE and liquid-condensed (LC) phases (LE-LC), to a LC phase at the high surface pressure. However, apart from the big difference in the cross-sectional area of the two lipids, the surface pressures of the LE-LC phase transitions are different, i.e. around ~8.0 mN/m for DPPG and ~13.5 mN/m for TMCL. This is due to the significant structural difference between them. Moreover, with increasing TMCL fraction, the isotherms

maintain similar shape, with the mean area per lipid molecule at a given surface pressure and the surface pressure of the phase transition shifting to higher values.

In the inset of Fig. 1a, the compressibility modulus of the mixture as a function of the DPPG molar fraction is shown for the three representative surface pressures of 8, 15 and 28 mN/m. According to the criterion given by Davies and Rideal [34] the modulus values vary from 10 to 50 mN/m for the LE phase and from 100 to 250 mN/m for the LC phase, while it rises above 250 mN/m for the solid phase (S). The compressibility modulus plot shows that the elastic properties of the mixtures undergo rather small variations with the composition, except for 15 mN/m, where the monolayer is close to the LE-LC phase transition, and with increasing the DPPG amount the monolayer becomes less compressible. Moreover, the elasticity of the monolayer decreases with increasing surface pressure, with the mixture being in the LE phase at 8 mN/m and in the LC phase at 28 mN/m.

In the case of the DPPG/DPPE mixture (Fig. 1b), increase in the amount of DPPE obliterates the LE state over low surface pressure region and the plateau region by lowering the mean area per lipid molecule of the mixture. As DPPE has a change of ~10% in the molecular area observed from 8 to 30 mN/m, the condensation over the low surface pressure region (< 8 mN/m) as observed between DPPG and DPPE should be conferred by DPPG. At the higher surface pressures of 15 and 28 mN/m, both DPPG and DPPE are in LC phases and their area per molecule values are comparable. However, at x_{DPPG} = 0.2 their average area per lipid molecule is higher than that of either the individual components, which then decreases with increasing the DPPE content. In the inset of Fig. 1b is also presented the compressibility modulus (surface elasticity) as a function of DPPG molar fraction. A decrease inelasticity is observed with increasing surface pressure and also with increasing the amount of DPPE, the monolayer becomes more condensed, even at lower surface pressures. Note that DPPE by itself has a very steep isotherm implying the poor compressibility of the lipids whereas DPPG has the well-defined LE, LE-to-LC and LC phases due to its charged nature.

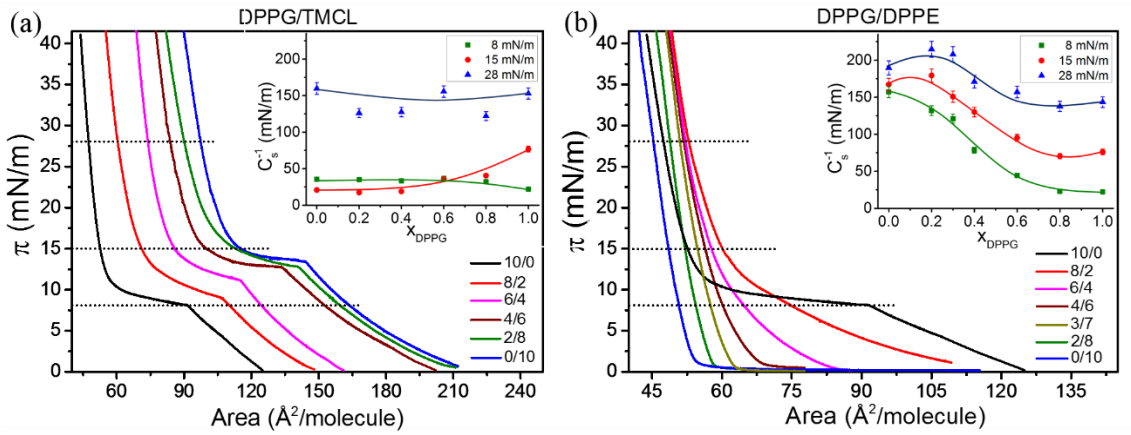

Fig. 1 Surface pressure-area (π-A) isotherms and compressibility modulus plots vs DPPG molar fraction (inset) for the (a) DPPG/TMCL and (b) DPPG/DPPE monolayers. The lines connecting the data points in the compressibility modulus plot are given as a guide to follow the trend of changes in the values of the modulus. The horizontal dashed lines indicate where the compressibility moduli were estimated.

In order to further analyse the lipid miscibility in the binary monolayer systems, the mean molecular areas of the DPPG/TMCL (Fig. 2a) and DPPG/DPPE (Fig. 2b) mixtures were plotted as a function of DPPG molar fraction for the three different surface pressures of 8, 15 and 28 mN/m, where the dashed line indicates the ideal mixing of the components. As it can be observed in Fig. 2a, the average molecular areas for the DPPG/TMCL mixtures at all surface pressures show positive deviations from the additivity rule, indicating the presence of repulsive interactions between the two lipid components in the monolayer mixtures. Moreover, the positive deviations in the excess molecular area plot against DPPG molar fraction (Fig. 2c) indicate that due to the lateral interactions between molecules, an expansion effect can be seen from all the surface pressures, with the extent of the deviation decreasing with the film compression. Interestingly, in the case of the DPPG/DPPE mixture, at the lowest surface pressure (8 mN/m) where the DPPG monolayer is in a chain-disordered LE phase, the mixture presented negative deviations, with the A_{ex} plot (Fig. 2d) indicating a condensation or attraction, implying that the two components must be well mixed. However, at the higher surface pressure values, this attractive force is diminished and repulsive interactions appear between the molecules, rendering the mixture less miscible.

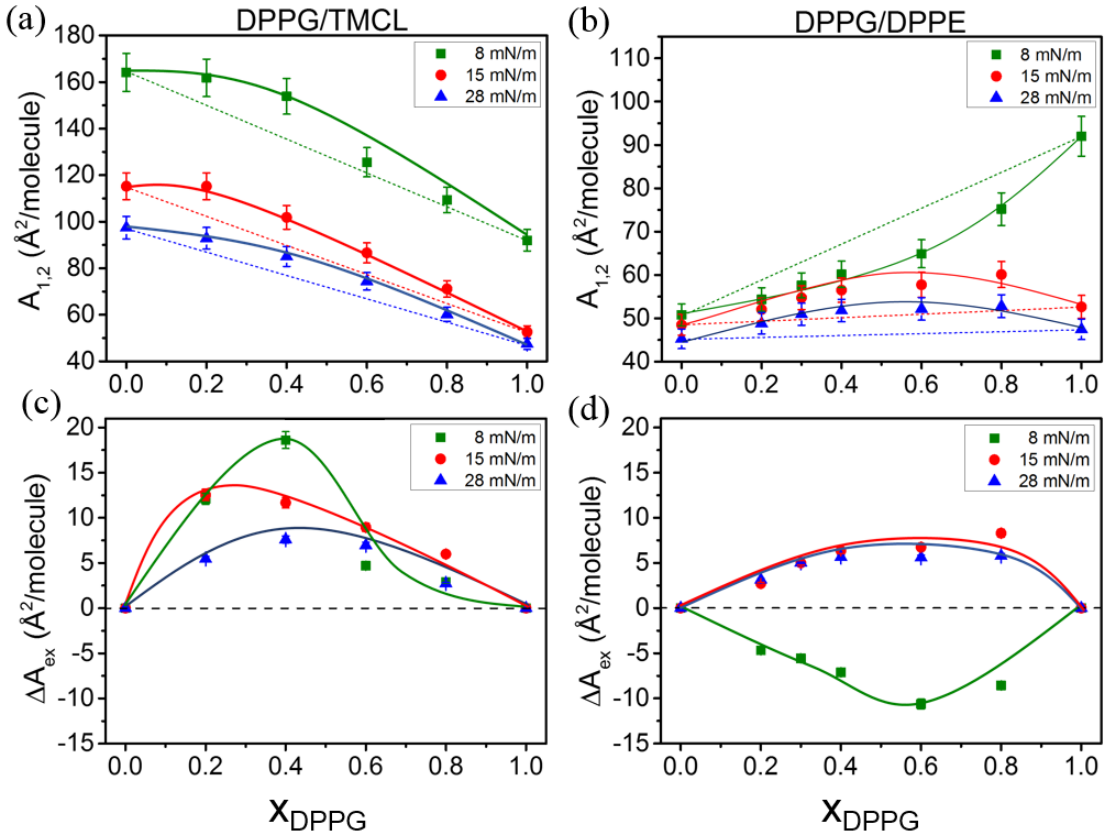

Fig. 2 The mean molecular areas, $A_{1,2}$, and excess molecular areas, ΔA_{ex}, versus DPPG molar fraction plots for the (a and c) DPPG/TMCL and (b and d) DPPG/DPPE monolayers. The points are exact values calculated from the given π values on the respective isotherms, with the curves serving as guidelines underlining the trend in the binary component monolayer.

Further information on the DPPG/TMCL and DPPG/DPPE interactions in the two mixed monolayers was acquired from the analysis of the excess Gibbs energy of mixing and the total free energy of mixing (Fig. 3). For all the three investigated surface pressures of the DPPG/TMCL mixture, the G_{ex} values are positive (Fig. 3a), again indicating strong repulsive interactions between the two components and tendency for phase separation in the monolayer; the higher the lipid packing, the more unstable is the monolayer. However, the negative values of the G_{mix} (Fig. 3c) for all the three surface pressures indicate that the mixed state is thermodynamically more stable than the corresponding unmixed state. In the case of the DPPG/DPPE mixture, the negative values of G_{ex} (Fig. 3b) for the surface pressure of 8 mN/m show that the interactions between the two lipids are more attractive than those of individual components, indicating greater stability of the mixed monolayer. However, for the two higher surface pressures, the strong repulsive interactions take over and the mixed monolayer undergoes phase separation. In what concerns the thermodynamic stability of the

mixtures, similar to the DPPG/TMCL mixtures, the G_{mix} plot of the DPPG/DPPE (Fig. 3d) monolayers shows a higher thermodynamic stability in the 2D mixed state than in the unmixed state. Moreover, the figure shows that the behaviour of the mixed monolayer system was thermodynamically favourable at low surface pressure, indicating more stable mixed monolayer formed under the condition.

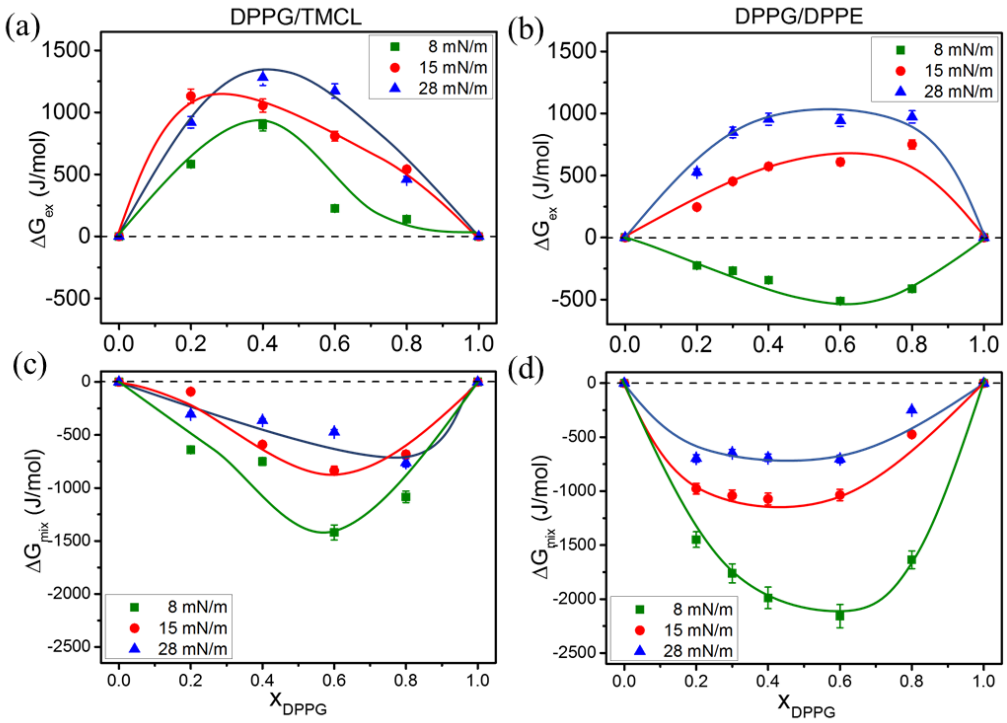

Fig. 3 The excess Gibbs energy of mixing, G_{ex}, and total free energy of mixing, G_{mix}, versus DPPG molar fraction plots for the (a and c) DPPG/TMCL and (b and d) DPPG/DPPE monolayers. The points are exact values calculated from the given π values on the respective isotherms, with the curves serving as guidelines underlining the trend in the binary component monolayer.

Based on the thermodynamic analysis of the two lipid mixtures, it can be concluded that both DPPG/TMCL and DPPG/DPPE systems are only partially miscible and form non-ideally mixed monolayers at the interface. However, the 2D mixed states are thermodynamically more stable than the corresponding unmixed states. Furthermore, as indicated by the minimum G_{mix} values, the higher thermodynamic stability of the two monolayers exists when the lipids are mixed near equimolar proportion and the stability decreases with increasing surface pressure. At the lower surface pressure the monolayers are more loosely organised and there is more freedom for the DPPE and TMCL molecules, respectively, to intermingle among the DPPG molecules. The increase in lateral pressure lowers the thermodynamic

stability of the condensed monolayers and the tendency for them to expand is observed. The observations are also consistent with the non-ideal mixing in which the individual lipids tend to interact among themselves to cause phase separation and form clusters.

Wydro et al [52] have conducted a similar study regarding the mixing behaviour of DPPG/DPPE monolayers. They found that at 32.5 mN/m the mixed monolayers are highly condensed. However, in their work they used pure water as subphase. Thus, condensation must arise from hydrogen bonding between glycerol hydroxyl groups and the phosphate groups of the neighbouring DPPG molecules, and the ammonium and phosphate groups of DPPE lipids, but PE is of course capable of forming hydrogen bonding with both PE and PG. In our work we used physiologically relevant buffer conditions (10 mM PBS, 137 mM NaCl, pH 7.4). It is well known that monovalent and divalent ions strongly affect the behaviour of charged Langmuir monolayers [53, 54]. For example, Suzuki and Matsushita [50] used cephalin (which primarily consists of PE and PS) to study the effect of metal ions on the isotherms. They found that monovalent and divalent ions expanded the lipid monolayer, due to the binding and association of these ions to the negatively charged sites (phosphoric and carboxylic groups) and formation of strong metal-phospholipid complexes, breaking the hydrogen bonding network in the pure water environment. Moreover, under these buffer conditions, DPPG head groups are deprotonated, and Na^+ ions screen the electrostatic interactions between neighbouring lipids. These observations help explain the non-ideal mixing behaviour and the phase separation between DPPG and DPPE lipids under the influence of added salts. However, at low surface pressures, where the DPPG monolayer is in the LE phase, apart from electrostatic interactions, hydrophobic interactions between the acyl chains also play a crucial role between the lipids. Thus, with the increase in DPPE amount under these conditions, the condensing effect became dominant due to the hydrogen bonding effect of DPPE. In the case of DPPG/TMCL mixtures, where both lipids are anionic, the significant structural differences between the two lipid components can contribute to the non-ideal mixing and phase separation.

3.2 Interaction with G_4 – surface pressure measurements

In order to mimic the G+ and G- bacterial membranes using binary component monolayers, and to study the binding of G_4, we have chosen DPPG/TMCL at the molar ratio of 6/4 as a model for the *S. aureus* membrane, and DPPG/DPPE at the molar ratio of 3/7 as an inner membrane model for *E. coli* [1]. Although the lateral pressure in the biological membranes is

often around 30 mN/m and the lipids are mainly in the fluid phase, we have chosen to examine G_4 binding from lower surface pressures to gain an understanding of the influence of membrane pressure change. We chose 15 mN/m as the initial pressure for G_4 binding study. Moreover, as we have studied the interaction of G_4 with single component monolayers at the same initial surface pressure, this will allow a direct comparison between the results.

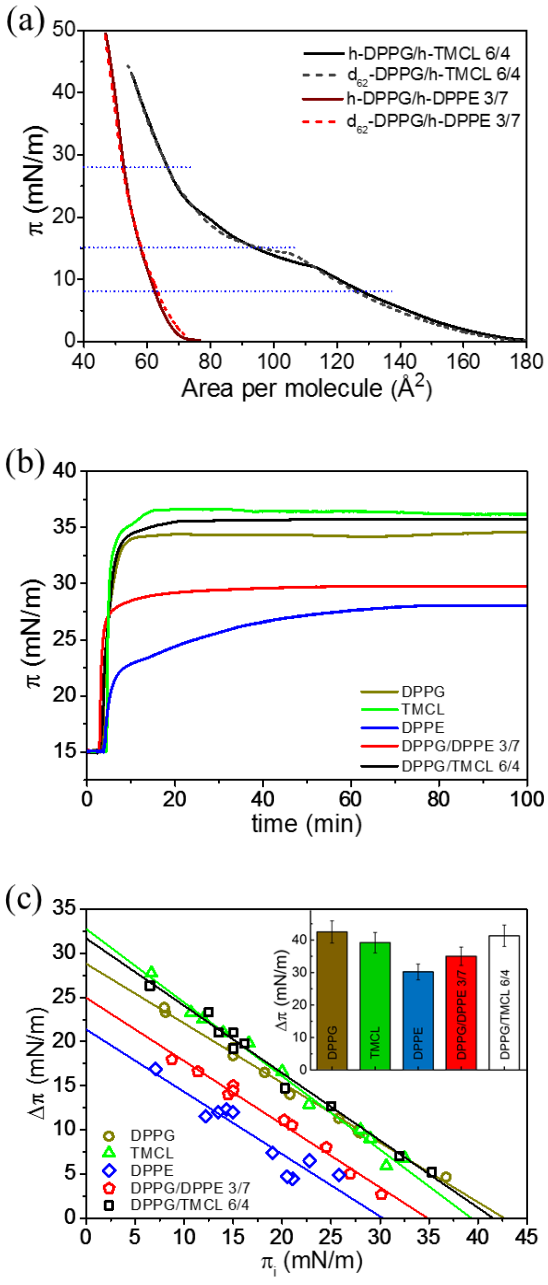

Fig. 4. (a) Surface pressure vs mean area per lipid molecule (π-A) isotherms for the hydrogenous and deuterated DPPG/TMCL (6/4) and DPPG/DPPE (3/7) monolayers; (b) binding kinetics after injection of G_4 at the initial surface pressure of 15 mN/m; and (c) plots of equilibrium surface pressure increase ($\Delta\pi$) following G_4 injection versus the initial surface pressure (π_i), and also shown in inset are the histograms of the MIP of G_4 calculated by regression of each $\Delta\pi$ vs π_i plot to the x axis.

As NR involves the use of hydrogenous (h-) and deuterated (d-) lipids, it is very important to characterise their behaviour first. Fig. 4a shows the π-A isotherms of the two isotopic analogues for the DPPG/TMCL (6/4) and DPPG/DPPE (3/7) systems, and the close similarity

indicates little isotopic effect associated with partial deuterium labelling to DPPG and its related binary mixtures. Fig. S2 further compares the π-A isotherms against individual component monolayers involving h- and d-DPPG. As already described, the DPPG/TMCL mixture presents well-defined phase transition behaviour, from LE to plateau and LC phases, while the DPPG/DPPE mixture has a steep curve, reaching the LC phase from low surface pressure values (< 1 mN/m). These curves have slightly different behaviour when compared with π-A isotherms from Fig. 1. The difference arises from the slightly different isotherm of the DPPG monolayer (slight batch to batch variation), with a shorter plateau region and a kink on the isotherm during the condensed phase, consistent with observations reported previously [31, 55].

The impact upon the injection of G_4 under mixed monolayers of DPPG/TMCL and DPPG/DPPE as a function of DPPG molar ratio at the initial surface pressure of 15 mN/m was measured by the change in surface pressure, $\Delta\pi = \pi_e - \pi_i$, where π_i is the initial surface pressures and π_e the equilibrium adsorption pressure. Fig. S3 shows how binary mixing affects the further surface pressure rise under these conditions. Changes in surface pressure are influenced by the association of G_4 to the lipid monolayers. Upon addition of G_4 under pure DPPG and TMLC monolayers, $\Delta\pi$ was ~20 mN/m, suggesting that although the two lipids are structurally very different, the main driving force of binding arises from charge interactions. When adding the G_4 under the DPPE monolayer, $\Delta\pi$ was 11 ± 2 mN/m, comparable with that observed for G_4 adsorption under DPPC monolayer (10 ± 2 mN/m) [31], and suggesting an entropic effect associated with the interfacial association.

Data on G_4 binding to the mixed DPPG/TMCL monolayers show that $\Delta\pi$ does not change with increasing starting surface pressure, whereas in the case of DPPG/DPPE mixture $\Delta\pi$ gradually increases with the increase of DPPG content in the lipid monolayer. The results on the binding of G_4 upon injection at the initial surface pressure of 15 mN/m under the mixed DPPG/TMCL (6/4) and DPPG/DPPE (3/7) monolayers are compared to those from the individual components as shown in Fig. 4b, with the kinetic G_4 binding processes resolved as the surface pressure changes over time. Each system reached its π_e within the first hour after G_4 injection, with the magnitude of the surface pressure change increasing with the amount of anionic lipid content. Then, in order to determine the maximum insertion pressure (MIP) of the monolayer to which G_4 can still insert into the monolayer, G_4 was injected at different π_i of the lipid monolayers, and the plot of the surface pressure increases as a function of π_i was drawn (Fig. 4c). The MIP for each system was then determined by extrapolating the

regression of the plot to x axis (shown as histograms in the inset of Fig. 4c). The lowest MIP value was calculated for DPPE (30.2 ± 2.5 mN/m), which then increases to 35 ± 2.8 when adding 30% DPPG in the layer. The MIP values for individual components, TMCL (39.2 ± 3 mN/m) and DPPG (42.5 ± 3 mN/m), as well as their 6/4 mixture (41.3 ± 3 mN/m), are well above the lateral pressure of the membrane, suggesting that the AMP molecules could steadily bind and penetrate the membranes. The different MIPs strongly support the role of membrane lipid composition in the binding of G_4 and exertion of its bactericidal activities.

3.3 NR studies

3.3.1 Kinetic compositional analysis during peptide binding

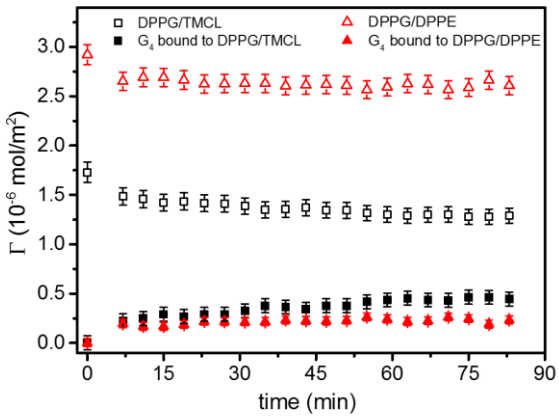

Fig. 5 Surface concentration values versus time showing the simultaneous binding of G_4 peptide to the interface of DPPG/TMCL (6/4) and DPPG/DPPE (3/7), together with the lipid loss, determined by the kinetic composition implementation of NR. At time 0, the surface concentrations of lipids were stable but upon peptide injection, some lipids were removed from surface monolayers whilst the peptide was co-adsorbed.

The low-*Q* analysis [31, 38-41] was adopted to gain information about the dynamic binding and compositional changes before and after injecting G_4 under the lipid monolayers at the initial surface pressure of 15 mN/m, with the results shown in Fig. 5. The error bars represent the uncertainty of the measurements, and were estimated to be 5% of the final lipid values, and 10% of the final peptide values. The DPPG/DPPE system has a higher initial surface concentration in μmol/m^2 than DPPG/TMCL. As explained previously, the molecular structure differs between DPPE and TMCL, and their mixing with DPPG leads to different behaviour and packing (Fig. 4a). Upon injection under both mixed lipid monolayers, similarly to our previous results on single component monolayers [31, 32], the peptide causes

fast removal of the lipids from the interface in the first 10 min whilst its co-adsorbed amount showed fast increase as well. Peptide binding and lipid removal subsequently slowed down and the processes tended to equilibration after about 60 min. DPPE is zwitterionic, but both DPPG and TMCL are negatively charged. Electrostatic interactions dominated the initial binding between the cationic G_4 and anionic lipids. The subsequent changes were much slower with far less increase in peptide adsorption or lipid loss, in good agreement with surface pressure measurements (Fig. 4b). Although the amount of lipids removed via G_4 initiated dissolution is 0.4–0.45 μmol/m^2, the relative fraction of the lipid removal is 0.13 from the binary DPPG/DPPE monolayer and 0.26 from the binary DPPG/TMCL monolayer.

3.3.2 Equilibrium structural analysis before peptide addition

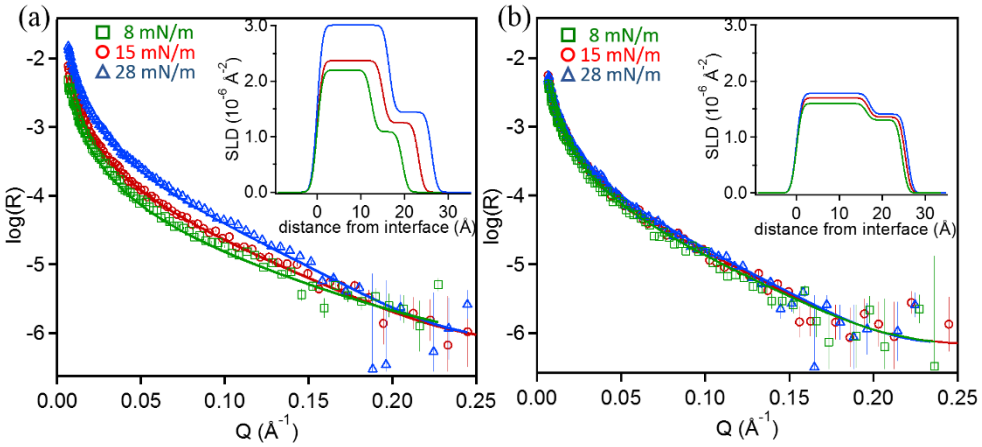

Fig. 6 Exemplar sets of neutron reflectivity profiles and the best 2-layer model fits (d-lipids on NRW) for (a) DPPG/TMCL; (b) DPPG/DPPE lipid monolayers at surface pressures of 8 (□), 15 (o), and 28 mN/m (Δ). The SLD profiles of the fits as a function of distance normal to the monolayer surface are represented in the insets, with the corresponding colours denoting SLD profile at the surface pressure of 8 (green), 15 (red) and 28 mN/m (blue), respectively.

The structural features of the binary component lipid monolayers mimicking G+ and G- bacterial membranes were determined by NR under 4 isotopic contrasts: h-lipid on NRW, d-lipid on NRW, h-lipid on D_2O and d-lipid on D_2O following sample equilibration. Complementing the thermodynamic analysis, the monolayers were characterised by NR at the initial surface pressures of 8, 15 and 28 mN/m. The reflectivity profiles were fitted using a two-layer model where the tails were in the first layer in air and the head groups distributed in the solvent-filled second layer. The model fits were made over the full *Q* range simultaneously to all 4 contrasts and the results are shown for all lipid structures associated with the different surface pressures in Fig. S4 for DPPG/TMCL (6/4) and Fig. S5 for

DPPG/DPPE (3/7) monolayers, with the associated best fitted values presented in Table S2 and Table S3. Fig. 6 shows exemplar sets of the fitted NR data and the associated SLD profiles for DPPG/TMCL (Fig. 6a) and DPPG/DPPE (Fig. 6b) monolayers involving d-lipids on NRW at the 3 surface pressures of 8, 15 and 28 mN/m. Table 1 and Table 2 summarise the main structural parameters obtained from the fits to the DPPG/TMCL and DPPG/DPPE monolayers, respectively. The errors indicate the range of sensitive changes in reflectivity beyond which visual deviations could be observed between the calculated and measured profiles (this applies to all subsequent tables, including those from the Support Information). Note that these errors were larger than the sum of statistical and fitting errors.

Table 1. Main structural parameters obtained from the best 2-layer model fits to the NR profiles for DPPG/TMCL monolayers at initial surface pressures of 8, 15, and 28 mN/m.

Layer	**τ (Å)**	**φ_{lipid}**	**$\varphi_{solvent}$**	**A_{lipid} (Å^2)**	**Γ_{lipid} (10^{-6} mol/m^2)**
π_i = 8 mN/m					
(1st) acyl chain	12.4 ± 1	0.68 ± 0.07	-	126 ± 9	1.31 ± 0.1
(2nd) head group	7.1 ± 0.5	0.40 ± 0.04	0.60 ± 0.06	126 ± 9	1.32 ± 0.1
π_i = 15 mN/m					
(1st) acyl chain	15.0 ± 1.5	0.73 ± 0.07	-	97 ± 7	1.72 ± 0.15
(2nd) head group	8.2 ± 0.6	0.46 ± 0.05	0.54 ± 0.05	95 ± 7	1.75 ± 0.15
π_i = 28 mN/m					
(1st) acyl chain	16.5 ± 1.5	0.93 ± 0.09	-	69 ± 5	2.39 ± 0.2
(2nd) head group	9.7 ± 0.7	0.53 ± 0.05	0.47 ± 0.05	69 ± 5	2.39 ± 0.2

Table 2. Main structural parameters obtained from the best 2-layer model fits to the NR profiles for DPPG/DPPE monolayers at initial surface pressures of 8, 15, and 28 mN/m.

Layer	**τ (Å)**	**φ_{lipid}**	**$\varphi_{solvent}$**	**A_{lipid} (Å^2)**	**Γ_{lipid} (10^{-6} mol/m^2)**
π_i = 8 mN/m					
(1st) acyl chain	16.3±1.5	0.81± 0.08	-	62 ± 5	2.70±0.21
(2nd) head group	8.3±0.6	0.50 ± 0.05	0.50 ± 0.05	60 ± 5	2.76±0.22
π_i = 15 mN/m					
(1st) acyl chain	16.8±1.5	0.87 ± 0.08	-	56 ± 4	2.94±0.25
(2nd) head group	8.6±0.6	0.52 ± 0.05	0.48 ± 0.05	56 ± 4	2.97±0.25
π_i = 28 mN/m					
(1st) acyl chain	17.3±1.5	0.91 ± 0.09	-	52 ± 4	3.17±0.26
(2nd) head group	9.0±0.7	0.54 ± 0.05	0.46 ± 0.05	51 ± 4	3.23±0.26

As seen from Fig. 6a, the associated data shown in Table 1 and the π-A isotherms shown in Fig. 1a and Fig. 4a, the DPPG/TMCL monolayer undergoes noticeable changes with the increase in surface pressure. At the lowest surface pressure, the monolayer is in the LE phase, the tails have a thickness of 12.4 Å with a volume fraction of 0.68 and a mean area per lipid molecule of ~126 Å^2, in good agreement with the mean area per lipid molecule measured

from the π-A isotherm (Fig. 4a). With the increase in surface pressure, the tail layer thickness increases to 15.0 Å at 15 mN/m and 16.5 Å at 28 mN/m, confirming changes in ordering and packing with rising compression. The mixed tail thicknesses are shorter than the average values of the theoretical thicknesses of the fully extended myristoyl tail of 19 Å [56], and of the palmitoyl chain ~23 Å [57], suggesting the acyl tails are bending away from the surface normal direction. In the meantime, the head group thickness has increased from 7.1 to 9.7 Å against the rising surface pressure, with their volume fraction increasing from 0.40 to 0.53. The mean area per lipid molecule dropped to 95 and 70 $Å^2$. In contrast, the DPPG/DPPE mixture had very different structural changes with surface compression. As shown in Fig. 6b, Table 2 and π-A isotherms from Fig. 4a, the monolayer is in the LC phase during all of the tested initial surface pressures. The tail thickness undergoes only small increase with surface pressure, from 16.3 to 17.3 Å, again indicating tilting away from the surface normal direction. Similarly, the head group thickness increases only by ~ 0.7 Å, i.e., from 8.3 Å to 9.0 Å, and the solvation decreases from 0.50 to 0.46. Thus, against the changes in the surface pressure, water number around the head groups of the binary DPPG/TMCL mixture decreased from 18 to 10, whilst that in the case of the DPPG/DPPE mixture changed little, from 8 to 7. The mean area per lipid molecule dropped from 62 to 55 and 51 $Å^2$, consistent with the more packed monolayers.

3.3.3 Equilibrium structural analysis after peptide binding

G_4 was subsequently injected under the monolayers at an initial surface pressure of 15 mN/m, and a structural analysis was conducted over the full *Q* range for data recorded in all 4 isotopic contrasts. On the basis of the 2-layer model used to fit the lipid-only systems, we have tried to fit each monolayer incorporating the G_4 peptide using a similar 2-layer model by allowing the peptide to penetrate both the tail (1^{st}) and solvated head group (2^{nd}) layers. The 2-layer model was satisfactory in the case of the DPPG/DPPE monolayer due to the low amount of the peptide associated with both tail and head group layers. However, fits to this model were found to be unsatisfactory for the DPPG/TMCL monolayer. It was found that to fit the 4 isotopic contrasts simultaneously an unrealistically high thickness had to be used for the 2^{nd} layer under water. Thus, a 3-layer model was utilised, with the 1^{st} layer containing the tails associated with the peptide in air, the 2^{nd} layer with solvated head groups and the peptide associated, and the 3^{rd} layer only with peptide and filled with solvent. Fig. 7 shows representative reflectivity profiles with the best fits for the DPPG/TMCL (Fig. 7a) and DPPG/DPPE (Fig. 7b) monolayers before and after G_4 addition with the associated SLD

profiles shown in the insets. The two isotopic contrasts are deuterated lipids on NRW and hydrogenous lipids on D_2O. The full set of 4 contrasts of the neutron reflectivity profiles (with and without G_4) together with their model fits are shown in Fig. S6. The main structural parameters obtained for the two systems are given in Table 3 (the thickness and SLD values are given in Table S4 and Table S5).

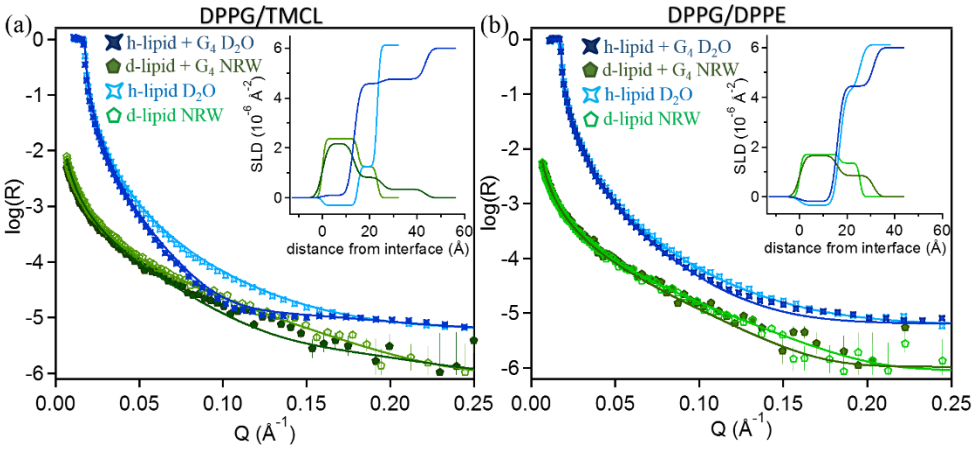

Fig. 7 Neutron reflectivity profiles with the best model fits for (a) DPPG/TMCL and (b) DPPG/DPPE monolayers after injection of G_4 at the initial surface pressure of 15 mN/m. The two isotopic contrasts are d-lipids on NRW and h-lipids on D_2O. The SLD profiles calculated from the best fits are plotted as a function of distance in the z-direction normal to the interface with the corresponding colours for each contrast shown in the inset kept the same as in the reflectivity profiles: d-lipid in NRW (green), d-lipid+G_4 in NRW (dark green), h-lipid in D_2O (light blue) and h-lipid+G_4 in D_2O (blue).

Table 3. Main structural parameters obtained from the best model fits for the DPPG/TMCL (6/4) and DPPG/DPPE (3/7) monolayers with G_4 bound under equilibration at the initial surface pressure of 15 mN/m.

Layer	**τ (Å)**	**φ_{lipid}**	**$\varphi_{peptide}$**	**$\varphi_{solvent}$**	**$A_{lipid\ end}$ (Å^2)**	**$\Gamma_{lipid\ end}$ (10^{-6} mol/m^2)**	**$\Gamma_{peptide}$ (10^{-6} mol/m^2)**
DPPG/TMCL							
(1st) acyl chain	13.3 ± 1	0.63±0.06	0.15 ± 0.01	-	128 ± 8	1.29 ± 0.10	0.11 ± 0.01
(2nd) head group	11.8 ± 1	0.24±0.02	0.17 ± 0.01	0.59 ± 0.05	128 ± 8	1.29 ± 0.10	0.12 ± 0.01
(3rd) peptide	18.3 ± 1.5	-	0.33 ± 0.03	0.67 ± 0.05	-	-	0.34 ± 0.02
DPPG/DPPE							
(1st) acyl chain	15.9 ± 1	0.82±0.08	0.06 ± 0.01	-	63.5 ± 4	2.62 ± 0.20	0.06 ± 0.01
(2nd) head group	15.2 ± 1	0.26±0.02	0.18 ± 0.02	0.56 ± 0.05	63.5 ± 4	2.62 ± 0.20	0.15 ± 0.01

Peptide binding to the DPPG/TMCL mixture induced changes across the entire interfacial layer, resulting in a decrease of the tail layer thickness from 15.0 to 13.5 Å and an increase of the head group layer thickness from 8.2 to 11.8 Å. The volume fractions of lipids in the layers also decreased, from 0.73 to 0.63 in the tail layer and from 0.46 to 0.24 for the head groups.

Across the monolayer, the volume fraction of the peptide was 0.15 in the 1st layer, 0.17 in the 2nd and 0.33 in the 3rd layer of 18.5 Å thick containing peptide only. From the final peptide surface concentration of 0.57 μmol/m^2, 19% was found in the tail layer (0.11 μmol/m^2), 20% in the head group layer (0.12 μmol/m^2), and the remaining 60% (0.34 μmol/m^2) distributed in the peptide-only layer.

In contrast, in the case of the DPPG/DPPE monolayer, the peptide did not induce considerable change to the interfacial layer. The thickness of the tail layer decreased only from 16.8 to 15.9 Å, with the lipid volume fraction decreasing by 6%. However, the thickness of the head group layer was found to be almost doubled, increasing from 8.6 Å to 15.6 Å. The volume fraction of the head group layer decreased from 0.52 to 0.26, with the volume fraction of the peptide being 0.18. The final peptide concentration was calculated to be 0.21 μmol/m^2, with 26% distributed in the tail region (0.06 μmol/m^2), while 74% in the head group region (0.15 μmol/m^2). It is thus clear that the amount of peptide bound and its distribution along the lipid monolayer were strongly influenced by lipid composition and their structural properties in the model monolayers.

3.4. Discussion

A very important step in deciphering the mechanism of action of AMPs is to understand how membrane composition and properties modulate peptide-lipid interactions and affect selectivity of the AMPs. The membrane composition varies between strain types and can also differ as an adaptive response to the living environment. The transport of antimicrobial agents across the cytoplasmic membrane of the cells is a very complex biological process, which, because of its dynamic nature, is very hard to study. The development of model lipid films to mimic some aspects of real biological membranes, in the form of either monolayers, bilayers, or multilayers, can facilitate a variety of techniques to unravel a wide range of information about biological membranes and their interactions with other bioactives such as AMPs.

Model spread lipid monolayers consisting of pure phosphatidylglycerols (DPPG or POPG), phosphatidylethanolamines (PEs), phosphatidylcholines (PCs), or Lipid A, have been used to study how different lipids discriminate the properties of AMPs [58-60]. Recent studies have focused on more complex mixtures of lipids, often represented by binary component models, using either PC/PG or more relevant PG/PE, and PG/CL with ratios (mol/mol or w/w) varying from 9:1, 3:1, or even 1:1 [61-63].

In this work, we have compared the structure of a G+ model monolayer consisting of DPPG/TMCL (6/4) and a G- model monolayer consisting of DPPG/DPPE (3/7) and their interactions with peptide G_4. From the combined surface pressure analysis and neutron reflectivity measurements, we observed that the greater strength of the G_4 peptide binding to the DPPG/TMCL monolayer was manifested by its stronger affinity to the full anionic lipid monolayer. Upon charge interaction, AMPs such as G_4 transform from non-ordered to α-helical structure [32], with the latter being significantly more amphiphilic and more potent at membrane binding and penetration. The charge interaction is followed by hydrophobic interaction and the interfacial binding processes must induce a great extent of G_4 transformation into the α-helical structure. The penetration of G_4 molecules into the acyl tail region causes structural disruptions to bacterial membranes.

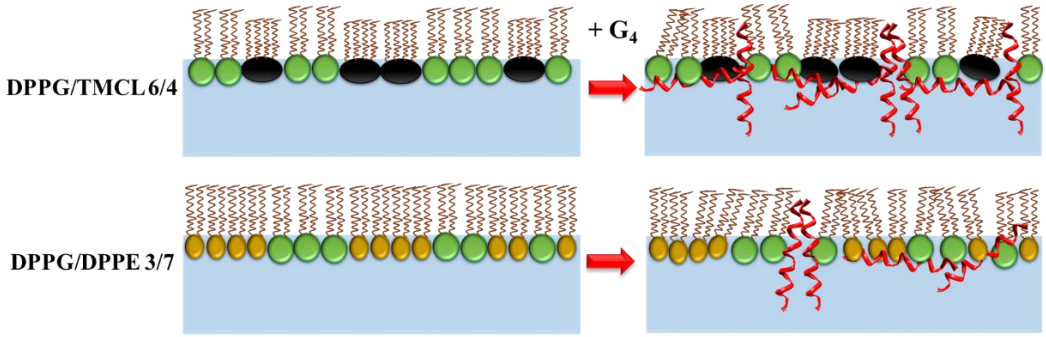

Fig. 8 Schematic representations of DPPG/TMCL and DPPG/DPPE monolayers without and with G_4 peptide bound across the interface.

Fig. 8 provides schematic depictions of the structural features of the binary lipid monolayers before and after G_4 binding. The unique structural characteristics as revealed from NR are the distributions of G_4 molecules across the model binary lipid membrane leaflets. G_4 is amphiphilic and its binding causes partial dissolution of some lipids, with a fraction of 0.26 of lipids removed from the DPPG/TMCL monolayer and 0.13 removed from the DPPG/DPPE monolayer. The higher fraction of lipids removal from the G+ bacterial membrane must be due to the full charges as well as the highly hydrophobic nature of the TMCL. The high extent of lipid removal together with the high extent of insertion of G_4 molecules into the model membrane leaflet, makes G_4 particularly potent at dislodging G+ bacterial membranes, an observation highly consistent with the experimental results from antimicrobial work where G_4 and related AMPs tend to make full killing of G+ bacteria such as *S. aureus* and *B. subtilis* with lower minimum inhibition concentrations than those from *E. coli* [33,64]. These observations are broadly consistent with the results from other models

involving pure lipid monolayers. Thus, the structural changes as observed from the binary lipid models in this work form a strong physical basis to correlate with the composition-dependent behaviour of AMPs and their antimicrobial potency [33,65].

Although the binary component lipid mixtures used in our current study are already complex in terms of feasible models to adopt NR, they still enable us to extract valuable information about structural changes. The merit of this work is to unravel how AMPs such as G_4 disrupt the main membrane leaflets surrounding G+ and G- bacteria. As indicated early, a technical advantage of the spread lipid monolayers over other more elaborate ones is the better use of NR resolution and control over surface pressure via Langmuir trough, important for studying this type of systems. Complementary studies are underway to examine how structural features such as the presence of lipopolysaccharides (LPS), another important component of the outer leaflet of the outer membrane from G- bacteria, can influence the binding and activity of AMPs such as G_4.

Conclusions

Lipid monolayers have been shown for more than one hundred years to be suitable models of membrane leaflets and can facilitate the application of a wide range of interfacial measurement techniques [3-5]. Following our previous studies of single component lipid monolayers by surface pressure and neutron reflectivity measurements [31, 32], this work has been extended to the binary component lipid monolayers composed of DPPG/TMCL and DPPG/DPPE, mimicking the membranes of G+ and G- bacteria. Surface pressure measurements revealed different molecular area changes in response to surface pressure variation due to different molecular structures including head group types and charges as well as the molecular shape. However, mixing within the lipid monolayers occurred non-ideally. Each binary system is shown to be only partially miscible yet thermodynamically more stable than the corresponding unmixed state with the highest stability occurring near equimolar lipid proportion. With increasing surface pressure, the monolayers became more condensed and more inclined to demix, resulting in the formation of lipid clusters in the film. The NR measurements of the binding of G_4 revealed stronger binding and penetration of the G_4 peptide to the DPPG/TMCL monolayer than to the DPPG/DPPE monolayer, consistent with the stronger electrostatic and hydrophobic interactions and more potent antimicrobial action on G+ bacteria. These results are also well correlated to the low haemolytic effect and strong antibacterial activity of cationic AMPs [21] [33] [64] and provide a clear physical basis that

helps to explain how AMPs disrupt membranes surrounding G+ and G- bacteria differently. This work has established more appropriate binary lipid membrane models for further developing AMPs that are more selective to G+ and G- bacteria, especially to pathogenic strains with known membrane composition.

Acknowledgements

The authors acknowledge support from a Marie Curie Fellowship ITN grant (grant number 608184) under SNAL (small nano-objects for alteration of lipid bilayers). We also acknowledge the awards of the neutron beam times on FIGARO at the ILL (https://dx.doi.org/10.5291/ILL-DATA.TEST-2552) on INTER (RB 1610224, Doi: 10.5286/ISIS.E.81735367) and SURF (RB 1520191, Doi: 10.5286/ISIS.E.73943720). We thank Simon Wood for assistance during the experiments at the ILL.

Author Contributions

DC: planned and carried out the experiments, analysed the data and wrote the manuscript. HG: contribution to neutron reflectivity experiments. RC, MC: the setup for neutron experiments, advice on data analysis and manuscript checking. HX: peptide synthesis and scientific insight in AMPs. JL: funding, research design, planning, supervising, manuscript writing and finalising.

References

[1] K. Lohner, Development of Novel Antimicrobial Agents: Emerging Strategies, Wymondham: Horizon Scientific Press, 2001.

[2] S. Reardon, Nature 513 (2014) 471.

[3] R. M. Epand, Biochim. Biophys. Acta 1462 (1999) 11-28.

[4] R. E. W. Hancock, H.-G. Sahl, Nat. Biotechnol. 24 (2006) 1551-1557.

[5] V. Teixeira, M. J. Feio M. Bastos, Prog. Lipid Res. 51 (2012) 149-177.

[6] C. Chen , J. Hu, C. Yang, Y. Zhang, F. Wang, Q. Mu, F. Pan, H. Xu, J. R. Lu, J. Mater. Chem. B 4 (2016) 2359-2368.

[7] D. Ciumac , H. Gong, X. Hu, J. R. Lu, J Colloid. Interf. Sci. 537 (2019) 163-185.

[8] J. Li, J.-J. Koh, S. Liu, R. Lakshminarayanan, C. S. Verma, R. W. Beuerman, Front. Neurosci. 11 (2017) 1-18.

[9] N. Malanovic, K. Lohner, Biochim. Biophys. Acta Biomembr. 1858 (2016) 936–946.

[10] L. A. Clifton, S. A. Holt, A. V. Hughes, E. L Daulton, W. Arunmanee, H. Frank, S. Khalid, D. Jefferies , T. R. Charlton, J. R. P. Webster, C. J. Kinane, J. H. Lakey, Angew. Chem. Int. Ed. 54 (2015) 11952–11955.

[11] L. A. Clifton, R. A. Campbell , F. Sebastiani, J. Campos-Terán, J. F. Gonzalez-Martinez, S. Björklund , J. Sotres, M. Cárdenas, Adv. Colloid Interface Sci. 277 (2020) 102118.

[12] G. Fragneto, R. Delhom, L. Joly, E. Scoppola, Curr. Opin. Colloid Interface Sci. 38 (2018) 108-121.

[13] C. Sohlenkamp, O. Geiger, FEMS Microbiol. Rev. 40 (2016) 133-159.

[14] R. M. Epand, R. F. Epand, Biochim. Biophys. Acta 1788 (2009) 289-294.

[15] Y. Kanemasa, Y. Akamatsu, S. Nojima , Biochim. Biophys. Acta 144 (1967) 382-390.

[16] R. P. H. Huijbregts, A. I. P. M. de Kroon, B. de Kruijff, Biochim. Biophys. Acta 1469 (2000) 43-61.

[17] A. Mrozik, Z. Piotrowska-Seget, S. Labuzek, Pol. J. Environ. Stud. 13 (2004) 487-494.

[18] R.S. Conrad, H.E. Gilleland Jr., J. Bacteriol. 148 (1981) 487-497.

[19] R. M. Epand, R. F. Epand, Mol. Biosyst. 5 (2009) 580-587.

[20] T. Koprivnjak, D. Zhang, C. M. Ernst, A. Peschel, W. M. Nauseef, J. P. Weiss, J. Bacteriol. 193 (2011) 4134–4142.

[21] R. M. Epand, S. Rotem, A. Mor, B. Berno, R. F. Epand, J. Am. Chem. Soc. 130 (2008)14346–14352.

[22] H. Zhao, P. Lappalainen, Mol. Biol. Cell. 23 (2012) 2823-2830.

[23] L. Yu, L. Guo, J. L. Ding, B. Ho, S. Feng, J. Popplewell, M. Swann, T. Wohland, Biochim. Biophys. Acta 1788 (2009) 333-344.

[24] N. Marín-Medina, D. A. Ramírez, S. Trier, C. Leidy, Appl. Microbiol. Biotechnol. 100, (2016) 10251-10263.

[25] H. Brockman, Curr. Opin. Struc. Biol. 9 (1999) 438-443.

[26] R. Maget-Dana, Biochim. Biophys. Acta 1462 (1999) 109-140.

[27] S. Feng, Langmuir, 15 (1999) 998-1010.

[28] D. Marsh, Biochim. Biophys. Acta 1286 (1996) 183-223.

[29] L. Zhang, A. Rozek, R. E. W. Hancock, J. Biol. Chem. 276 (2001) 35714–35722.

[30] E. Sevcsik, G. Pabst, W. Richter, S. Danner, H. Amenitsch, K. Lohner, Biophys. J. 94 (2008) 4688-4699.

[31] D. Ciumac, R. A. Campbell, H. Xu, L. A. Clifton, A. V. Hughes, J. R. P. Webster, J. R. Lu, Colloids Surf. B 150 (2017) 308-316.

[32] D. Ciumac, R. A. Campbell, L. A. Clifton, H. Xu, G. Fragneto, J. R. Lu, ACS Omega, 2 (2017) 7482-7492.

[33] J. Hu, C. Chen, S. Zhang, H. Xu, X. Zhao, J. R. Lu, Biomacromolecules 12 (2011) 3839-3843.

[34] J. T. Davies, E. K. Rideal, Interfacial Phenomena, New York and London: Academic Press, 1963.

[35] I. S. Costin, G. T. Barnes, J. Colloid Interface Sci. 51 (1975) 106-121.

[36] K. K. P. Dynarowicz-Łatka, K. Kita, Adv. Colloid Interface Sci. 79 (1999) 1-17.

[37] R. A. Campbell, H. P. Wacklin, I. Sutton, R.Cubitt, G.Fragneto, Eur. Phys. J. Plus.126 (2011) 107.

[38] L. Braun, M. Uhlig, R. von Klitzing, R. A. Campbell, Adv. Colloid Interface Sci. 247 (2017) 130-148.

[39] R. A. Campbell, Curr. Opin. Colloid Interface Sci. 37 (2018) 49-60.

[40] R. A. Campbell, A. Tummino, B. A. Noskov, I. Varga, Soft Matter 12 (2016) 5304-5312.

[41] A. Tummino, J. Toscano, F. Sebastiani, B. A. Noskov, I. Varga, R. A. Campbell, Langmuir 34 (2018) 2312-2323

[42] A. Nelson, J. Appl. Cryst. 39 (2006) 273-276.

[43] M. Born, E.Wolf, Principles of Optics, Oxford: Pergamon Press, 1970.

[44] O. S. Heavens, Optical Properties of Thin Solid Films, London: Butterworths, 1955.

[45] J.M. Boggs, Biochim. Biophys. Acta Biomembr. 906 (1987) 353–404.

[46] R.M. Epand, S.W. Hui, FEBS Lett. 209 (1986) 257–260.

[47] R.N. Lewis, R.N. McElhaney, Biochim. Biophys. Acta Biomembr. 1788 (2009) 2069–2079.

[48] M. Kates, J.-Y Syz, D. Gosser, T. H. Haines, Lipids 28 (1993) 877-882.

[49] R.P. Rand, S. SenGupta, Biochim. Biophys. Acta Biomembr. 255 (1972) 484–492.

[50] Y.Suzuki, H. Matsushita, Ind. Health 6 (1968) 128-133.

[51] J. J. G. Casares, L. Camacho, M. T. Martín-Romero, J. J. L. Cascales, ChemPhysChem. 9, (2008) 2538-2543.

[52] P. Wydro, M. Flasiński, M. Broniatowski, Biochim. Biophys. Acta 1818 (2012) 1745–1754.

[53] E. Leontidis, M. Christoforou, C. Georgiou, T. Delclos, Curr. Opin. Colloid Interface Sci. 19 (2014) 2-8.

[54] P. Koelsch, P. Viswanath, H. Motschmann, V. L. Shapovalov, G. Brezesinski, H. Mçhwald, D. Horinek, R. R. Netz, K. Giewekemeyer, T. Salditt, H. Schollmeyer, R. von Klitzing, J. Daillant, P. Guenoun, Colloid Surf, A: Physicochem. Eng. Aspects 303 (2007) 110–136.

[55] D. Grigoriev, R. Krustev, R. Miller, U. Pison, J, Phys, Chem. B 103 (1999) 1013-1018.

[56] A. P. Le Brun, L. A. Clifton, C. E. Halbert, B. Lin, M. Meron, P. J. Holden, J. H. Lakey, S. A. Holt, Biomacromolecules 14 (2013) 2014−2022.

[57] F. Miano, X. Zhao, J. R Lu, J. Penfold, Biophys. J. 92 (2007) 1254−1262.

[58] R. Volinsky, S. Kolusheva, A. Berman, R. Jelinek , Biochim. Biophys. Acta 1758 (2006) 1393-1407.

[59] F. Neville, C. S. Hodges, C. Liu, O. Konovalov, D. Gidalevitz, Biochim. Biophys. Acta (2006) 1758, 232-240.

[60] F. Neville, M. Cahuzac, O. Konovalov, Y. Ishitsuka, K. Y. C. Lee, I. Kuzmenko, G. M. Kale, D. Gidalevitz, Biophys. J 90 (2006) 1275-1287.

[61] I. Knyght, L. Clifton, Y. Saaka, M. J. Lawrence, D. J. Barlow, Langmuir 32 (2016) 7403-7410.

[62] A. Arouri, A. Kerth, M. Dathe, A. Blume, Langmuir 27 (2011) 2811-2818.

[63] A. Erbe, A. Kerth, M. Dathe, A. Blume, ChemBioChem. 10 (2009) 2884-2892.

[64] C. Chen, C. Yang , Y. Chen, F. Wang, Q. Mu, J. Zhang, Z. Li, F. Pan, H. Xu and J. R. Lu, ACS Appl. Mater. Inter. 8 (2016) 26501−26510.

[65] H.N. Gong, J. Zhang, X.X. Hu, Z.Y. Li, K. Fa, H.N. Liu, T.A. Waigh, A. McBain, J.R. Lu, ACS Appl. Mater. Inter. 11(2019) 34609-20.

Supporting Information

Structural elucidation upon binding of antimicrobial peptides into binary mixed lipid monolayers mimicking bacterial membranes

Daniela Ciumac[1], Haoning Gong[1], Richard A. Campbell[2,3], Mario Campana[4], Hai Xu[5] and Jian R. Lu[1,*]

[1] Biological Physics Laboratory, School of Physics and Astronomy, University of Manchester, Oxford Road, Schuster Building, Manchester M13 9PL,

[2] Institut Laue-Langevin, 71 Avenue des Martyrs, CS-20156, 38042 Grenoble, France

[3] Division of Pharmacy and Optometry, University of Manchester, Oxford Road, Stopford Building, Manchester M13 9PT.

[4] ISIS Neutron Facility, STFC, Chilton, Didcot OX11 0QZ, UK

[5] Centre for Bioengineering and Biotechnology, China University of Petroleum, Qingdao, China

* To whom all correspondence should be made; Tel: +44 161 2003926; Email: j.lu@manchester.ac.uk

S1. Molecular structures of the studied lipids

Molecular structures of the studied lipids are showed in Fig. S1, with the discussion on the differences between them presented in the main text.

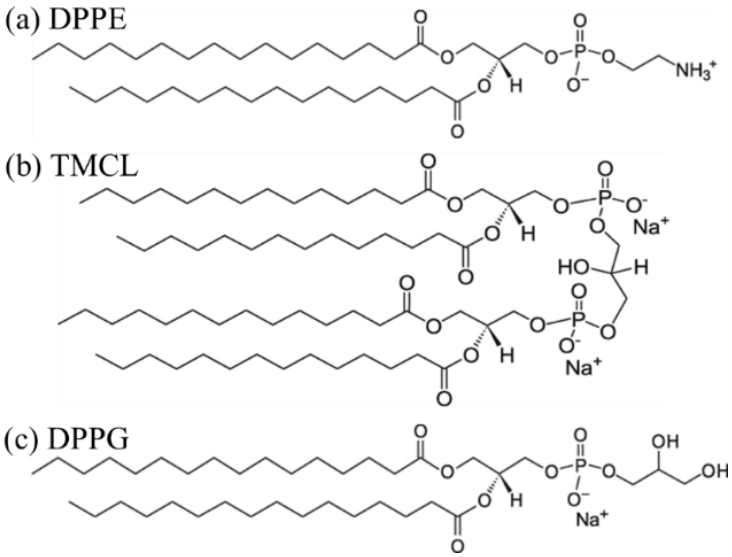

Fig. S1. Molecular structures of the lipids studied.

S2. SLD values of materials used in NR measurements

The SLD values and molecular volumes of all materials used in this study are summarised in Table S1. The volumes were estimated by adding the constituting segments by referring to the references as listed below (references [a], [b], and [c]).

Table S1. The scattering lengths (Σb), scattering length densities (ρ) and molecular volumes of the components of the individual key lipids and G_4 peptide (a) and the binary lipid mixture (b), where the tail refers to the two acyl chains in each lipid and the head refers to the respective lipid head group, and h and d refer to hydrogenous or deuterated fragment.

(a)

Component		**Scattering length ($\times10^{-5}$ Å)**	**Scattering length density ($\times10^{-6}$ Å^{-2})**	**Volume (Å^3)**
DPPG	whole molecule (h)	39.1	0.35	1105
	whole molecule (d_{62})	684.6	6.2	1105
	tails (h)	-32.5	-0.4	822
	tails (d_{62})	613.0	7.45	822
	head group (h)	71.5	2.5	283
DPPE	whole molecule (h)	30.1	0.3	1058
	tails (h)	-32.5	-0.4	822
	head group (h)	62.6	2.6	236
TMCL	whole molecule (h)	74.1	0.4	1891
	tails (h)	-58.3	-0.4	1425
	head group (h)	135.5	2.9	466.5
G_4 in NRW	$G(IIKK)_4I\text{-}NH_2$	301.3	1.02	2966
G_4 in D_2O	$G(IIKK)_4I\text{-}NH_2$	663.4	2.24	2966

(b)

Component		**Scattering length ($\times10^{-5}$ Å)**	**Scattering length density ($\times10^{-6}$ Å^{-2})**	**Volume (Å^3)**
DPPG/DPPE (3/7)	whole molecule (h/h)	32.8	0.3	1072.1
	whole molecule (d/h)	226.4	2.1	1072.1
	tails (h/h)	-32.5	-0.4	822
	tails (d/h)	161.2	1.96	822
	head group (h/h)	65.2	2.6	250.1
DPPG/TMCL (6/4)	whole molecule (h/h)	51.9	0.4	1419.6
	whole molecule (d/h)	440.4	3.1	1419.6
	tails (h/h)	-42.8	-0.4	1063.2
	tails (d/h)	344.5	3.2	1063.2
	head group (h/h)	97.1	2.7	356.2

S3. Surface pressure measurements

Fig. S2 shows the *π-A* isotherms of individual and binary mixed lipid monolayers for hydrogenous and deuterated DPPG, hydrogenous DPPE, hydrogenous TMCL and the related binary mixtures between d- and h-DPPG and h-DPPE and h-TMCL underpinning neutron reflection measurements.

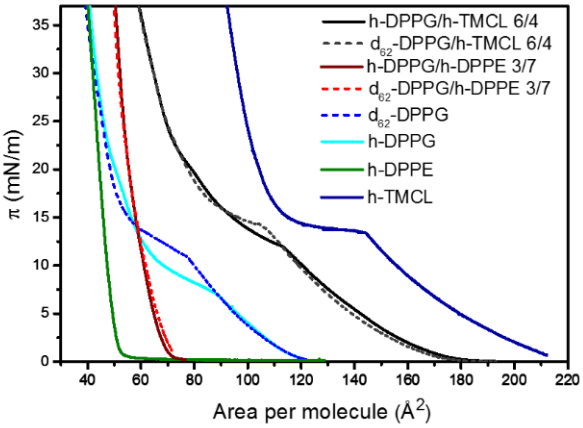

Fig. S2 The π-A isotherms of individual and binary component monolayers covering hydrogenous and deuterated DPPG and the related mixtures, which were used for the NR measurements.

Fig. S3 shows the changes in the surface pressure (Δπ) as a function of DPPG molar ratio upon addition of G_4 peptide to binary lipid monolayers made of DPPG/TMCL and DPPG/DPPE at the initial surface pressure of 15 mN/m, with the final peptide concentration in the subphase of 3 μM.

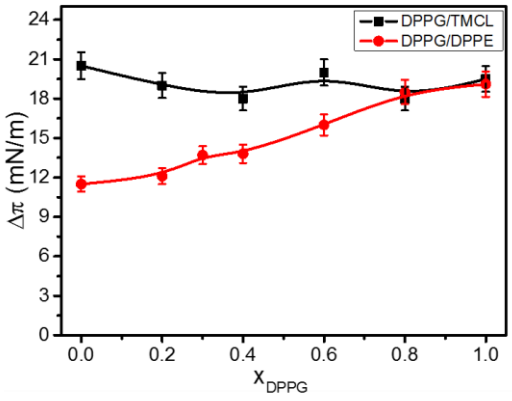

Fig. S3. Changes in the surface pressure (Δπ) under different DPPG molar ratios upon addition of G_4 peptide to binary lipid monolayers comprised of DPPG/TMCL and DPPG/DPPE at the initial surface pressure of 15 mN/m, with the final peptide concentration in the subphase of 3 μM. The lines are for guidance.

S4. Low *Q* analysis

The established low-*Q* analysis approach involves calculation of the product of the SLD and thickness of a single uniform layer that results from the scattering contributions (< 0.03 $Å^{-1}$) of two interfacial components in two isotopic contrasts (references [d] and [e]). These calculations are then used to resolve the surface concentrations of the two components through solving two linear equations. In the present case, there are three interfacial components, but the stoichiometry of the two lipid components spread at the interface is known, so the assumption is made that this ratio remains constant, hence the surface concentrations of three components can be resolved from two isotopic contrasts. In this case, an arbitrary fixed thickness of 21 Å was used in the model; the chosen thickness has minimal impact on the product as long as it is not so large that it changes the gradient of the fit.

To resolve the time-dependent peptide binding to the mixed lipid monolayers, the reflectivity data from the spread h/h lipid monolayers on NRW were measured every 4 min. For the monolayers with the d/h lipid contrast on NRW, where the signal is dominated by the deuterated lipids, thus making it hard to follow the binding dynamics, intermediate values were interpolated by applying a logarithmic fitting procedure to the scattering contributions from the interfacial components before and after the interaction. The low-*Q* analysis was applied to the lipids-only data (before peptide addition) and the resulting surface concentration of the adsorbed peptide was < 0.002 $\mu mol/m^2$, which validates the approach.

S5. Full *Q* analysis

Note that in the full *Q*-range analysis of the neutron reflectivity data, in order to reduce the differences between the model fit and the experimental data, the fitting parameters were adjusted by a least square minimisation procedure. A roughness value of 1 Å was used to fit the interfaces of the lipid-only layers and 2 Å to fit those of the layers containing the peptide.

Fig. S4 and Fig. S5 show the best model fits to the measured reflectivity data from both DPPG/TMCL and DPPG/DPPE monolayers at initial pressures of 8, 15 and 28 mN/m. The thickness and SLD values for the best 2-layer model are given in Table S2 for DPPG/TMCL and in Table S3 for DPPG/DPPE mixtures. The structural parameters obtained from the fits are summarised in Table 1 and Table 2 in the main text.

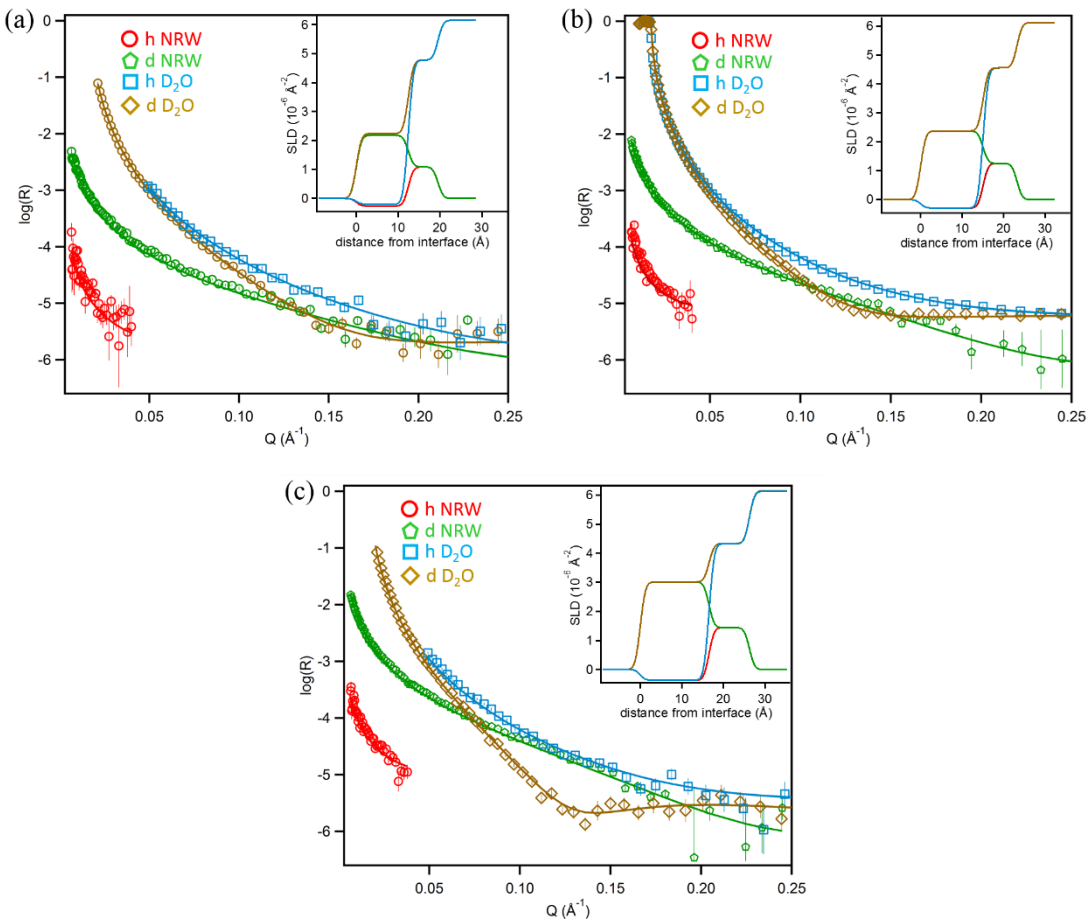

Figure S4. Neutron reflectivity profiles for DPPG/TMCL monolayers at (a) 8, (b) 15 and (b) 28 mN/m involving hydrogenous lipids (h-lipids) on NRW, chain-deuterated lipids (d-lipids) on NRW, h-lipids on D_2O and d-lipids on D_2O. The simultaneous two-layer fits are shown as solid lines with matching colours for each contrast. The SLD profiles obtained from the fits as a function of distance along the interface normal are plotted with the corresponding colours for each contrast.

Table S2. Best fitted structural parameters from the 2-layer model for the DPPG/TMCL monolayers at the initial surface pressures of 8, 15 and 28 mN/m.

Pressure	**Contrast**	**Fit parameters**	
		τ (Å)	**ρ (×10^{-6} Å^{-2})**
8 mN/m	Tails		
	h-DPPG/TMCL	12.4 ± 0.8	-0.27 ± 0.03
	d-DPPG/TMCL	12.4 ± 0.8	2.20 ± 0.20
	Head		
	DPPG/TMCL NRW	7.1 ± 0.5	1.09 ± 0.09
	DPPG/TMCL D_2O	7.1 ± 0.5	4.78 ± 0.45
15 mN/m	Tails		
	h-DPPG/TMCL	15 ± 1.4	-0.29 ± 0.03
	d-DPPG/TMCL	15 ± 1.4	2.37 ± 0.20
	Head		
	DPPG/TMCL NRW	8.2 ± 0.6	1.25 ± 0.10
	DPPG/TMCL D_2O	8.2 ± 0.6	4.56 ± 0.45
28 mN/m	Tails		
	h-DPPG/TMCL	16.5 ± 1.5	-0.37 ± 0.03

d-DPPG/TMCL	16.5 ± 1.5	3.01 ± 0.28
Head		
DPPG/TMCL NRW	9.7 ± 0.7	1.44 ± 0.10
DPPG/TMCL D_2O	9.7 ± 0.7	4.33 ± 0.40

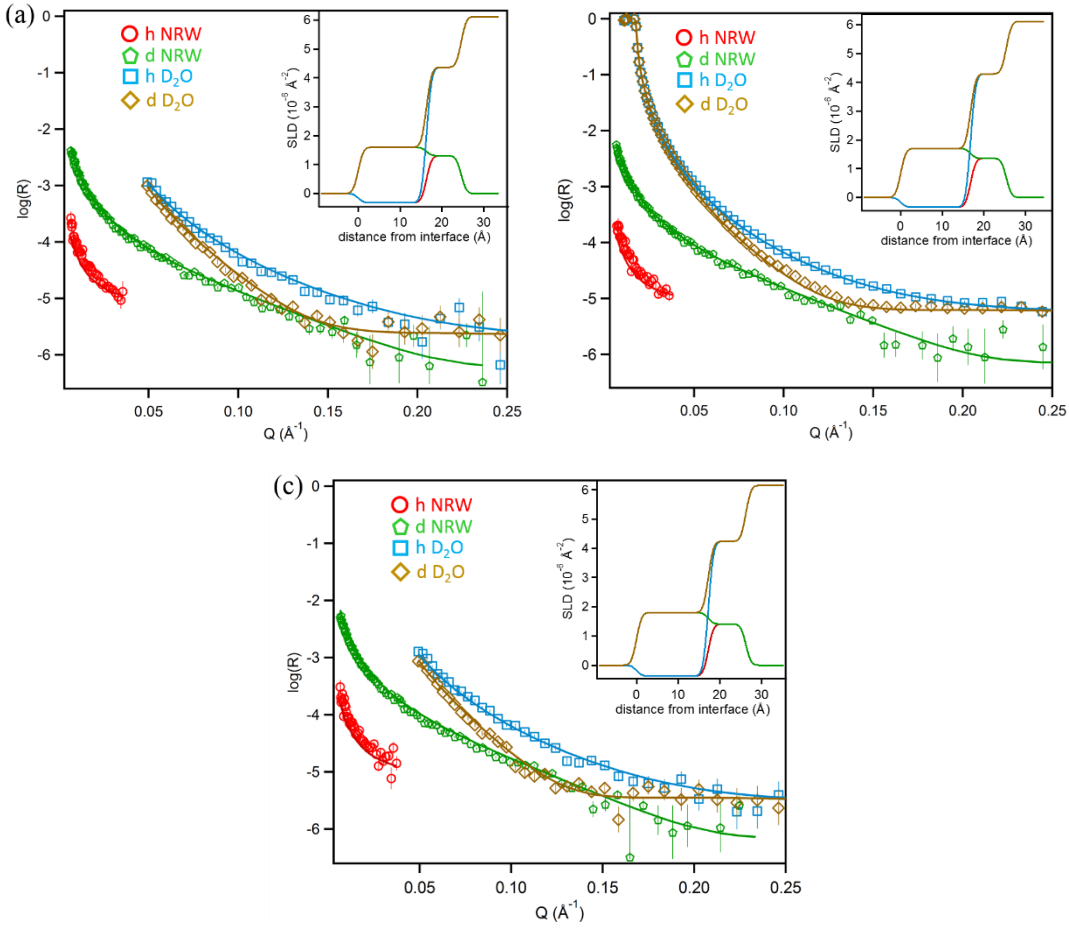

Figure S5. Neutron reflectivity profiles for DPPG/DPPE monolayers at (a) 8, (b) 15 and (c) 28 mN/m involving hydrogenous lipids (h-lipids) on NRW, chain-deuterated lipids (d-lipids) on NRW, h-lipids on D_2O and d-lipids on D_2O. The simultaneous two-layer fits are shown as solid lines with matching colours for each contrast. The SLD profiles obtained from the fits as a function of distance along the interface normal are plotted with the corresponding colours for each contrast.

Table S3. The best fitted structural parameters obtained from the 2-layer model for the DPPG/DPPE monolayers at the initial surface pressures of 8, 15 and 28 mN/m.

Pressure	**Contrast**	**Fit parameters**	
		τ (Å)	**ρ (×10^{-6} Å^{-2})**
8 mN/m	Tail		
	h-DPPG/DPPE	16.3 ± 1.4	-0.32 ± 0.03
	d-DPPG/DPPE	16.3 ± 1.4	1.60 ± 0.15

	Head		
	DPPG/DPPE NRW	8.3 ± 0.6	1.30 ± 0.10
	DPPG/DPPE D_2O	8.3 ± 0.6	4.36 ± 0.40
15 mN/m	Tail		
	h-DPPG/DPPE	16.8 ± 1.4	-0.34 ± 0.03
	d-DPPG/DPPE	16.8 ± 1.4	1.70 ± 0.16
	Head		
	DPPG/DPPE NRW	8.6 ± 0.6	1.36 ± 0.10
	DPPG/DPPE D_2O	8.6 ± 0.6	4.29 ± 0.40
28 mN/m	Tail		
	h-DPPG/DPPE	17.3 ± 1.5	-0.36 ± 0.04
	d-DPPG/DPPE	17.3 ± 1.5	1.78 ± 0.15
	Head		
	DPPG/DPPE NRW	9.0 ± 0.09	1.41 ± 0.10
	DPPG/DPPE D_2O	9.0 ± 0.09	4.22 ± 0.40

Figure S6 shows neutron reflectivity profiles and the best model fit to data for DPPG/TMCL 6/4 and DPPG/DPPE 3/7 monolayers after injection of 3 μM G_4 at the initial surface pressure of 15 mN/m. In the inset are shown the SLD profiles calculated from the fit as a function of the interface in the z-direction. The thickness and SLD values obtained from the best fit are given in Tables S4 and S5, and the associated structural parameters are given in Table 3.

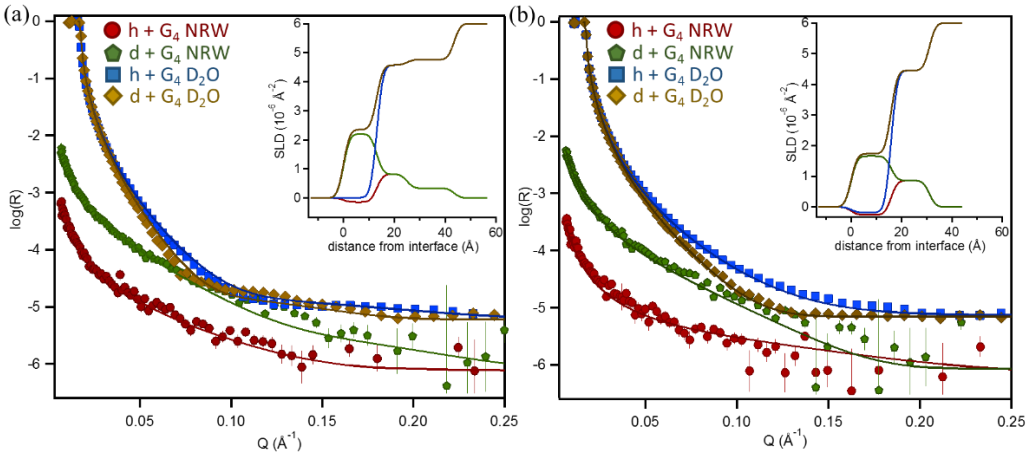

Figure S6. Neutron reflectivity profiles and the best model fit to data for (a) DPPG/TMCL 6/4 and (b) DPPG/DPPE 3/7 monolayers after injection of 3 μM G_4 at initial surface pressure of 15 mN/m. The profiles of the SLD calculated from the fit as a function of the interface in the z-direction with the corresponding colours for each contrast are shown in the inset. The thickness and SLD fit values are given in Tables S4 and S5, and the structural parameters used to obtain the best fit are given in Table 3.

Table S4. The best fitted structural parameters from the 3-layer model for the equilibrated G_4 binding onto the DPPG/TMCL 6/4 monolayers at the initial surface pressure of 15 mN/m.

Contrast	**Fit parameters**	
	τ (Å)	**ρ (×10^{-6} Å^{-2})**

(1^{st}) acyl chain		
h-DPPG/TMCL on NRW	13.3 ± 0.9	-0.10 ± 0.01
d-DPPG/TMCL on NRW	13.3 ± 0.9	2.17 ± 0.17
hDPPG/TMCL on D_2O	13.3 ± 0.9	0.10 ± 0.01
d-DPPG/TMCL on D_2O	13.3 ± 0.9	2.40 ± 0.17
(2^{nd}) head group		
DPPG/CL on NRW	11.8 ± 0.8	0.82 ± 0.08
DPPG/CL on D_2O	11.8 ± 0.8	4.57± 0.40
(3^{rd}) peptide		
G_4 in NRW	18.3 ± 2	0.34 ± 0.03
G_4 in D_2O	18.3 ± 2	4.76 ± 0.46

Table S5. The best fitted structural parameters from the 3-layer model for the equilibrated G_4 binding onto the DPPG/DPPE 3/7 monolayers at the initial surface pressure of 15 mN/m.

Contrast	**Fit parameters**	
	τ (Å)	**ρ ($\times 10^{-6}$ Å^{-2})**
(1^{st}) acyl chain		
h-DPPG/DPPE on NRW	15.9 ± 1.2	-0.26 ± 0.03
d-DPPG/DPPE on NRW	15.9 ± 1.2	1.66 ± 0.15
hDPPG/DPPE on D_2O	15.9 ± 1.2	-0.18 ± 0.02
d-DPPG/DPPE on D_2O	15.9 ± 1.2	1.74 ± 0.15
(2^{nd}) head group		
DPPG/DPPE on NRW	15.2 ± 1.1	0.86 ± 0.09
DPPG/DPPE on D_2O	15.2 ± 1.1	4.45 ± 0.40

References

[a] R. S. Armen, O. D. Uitto, S. E Feller, Biophys. J. 75 (1998) 734–744.
[b] N. Kučerka, B. W. Holland, C. G. Gray, B. Tomberli, J. Katsaras, J. Phys. Chem. B. 116 (2012) 232–239.
[c] J. Pan, F. A. Heberle, S. Tristram-Nagle, M. Szymanski, M. Koepfinger, J. Katsaras, N. Kučerka, Biochim. Biophys. Acta. 1818 (2012) 2135-2148.
[d] R. A. Campbell, A. Tummino, B. A. Noskov, I. Varga, Soft Matter 12 (2016) 5304-5312.
[e] L. Braun, M. Uhlig, R. von Klitzing, R. A. Campbell, Adv. Colloid Interface Sci. 247 (2017) 130-148.